

1 **A Comparative Study of Two-way and**
2 **Offline Coupled WRF v3.4 and CMAQ v5.0.2**
3 **over the Contiguous U.S.: Performance**
4 **Evaluation and Impacts of Chemistry-**
5 **Meteorology Feedbacks on Air Quality**

6 Kai Wang¹, Yang Zhang^{1*}, Shaocai Yu^{2*}, David C. Wong³, Jonathan Pleim³, Rohit Mathur³,
7 James T. Kelly⁴, and Michelle Bell⁵

8 ¹Department of Civil and Environmental Engineering, Northeastern University, Boston, MA
9 02115

10 ²Key Laboratory of Environmental Remediation and Ecological Health, Ministry of Education;
11 Research Center for Air Pollution and Health, College of Environment and Resource Sciences,
12 Zhejiang University, Hangzhou, Zhejiang 310058, P.R. China

13 ³Center for Environmental
14 Measurement and Modeling, U.S. EPA, RTP, NC 27711

15 ⁴Office of Air Quality Planning and Standards, U.S. EPA, RTP, NC 27711

16 ⁵School of Forestry & Environmental Studies, Yale University, New Haven, CT 06511

17

18 **Correspondence to:* Yang Zhang (ya.zhang@northeastern.edu); Shaocai Yu (shaocaiyu@zju.edu.cn)

19

20 **Abstract**

21 The two-way coupled Weather Research and Forecasting and Community Multiscale Air
22 Quality (WRF-CMAQ) model has been developed to more realistically represent the atmosphere
23 by accounting for complex chemistry-meteorology feedbacks. In this study, we present a
24 comparative analysis of two-way (with consideration of both aerosol direct and indirect effects)
25 and offline coupled WRF v3.4 and CMAQ v5.0.2 over the contiguous U.S. Long-term (five-year
26 of 2008-2012) simulations using WRF-CMAQ with both offline and two-way coupling modes
27 are carried out with anthropogenic emissions based on multiple years of the U.S. National
28 Emission Inventory and chemical initial and boundary conditions derived from an advanced
29 Earth system model (i.e., a modified version of the Community Earth System Model/Community
30 Atmospheric Model). The comprehensive model evaluations show that both two-way WRF-
31 CMAQ and WRF-only simulations perform well for major meteorological variables such as
32 temperature at 2 m, relative humidity at 2 m, wind speed at 10 m, and precipitation (except for
33 against the National Climatic Data Center data) as well as shortwave/longwave radiation. Both
34 two-way and offline CMAQ also show good performance for ozone (O₃) and fine particulate
35 matter (PM_{2.5}). Due to the consideration of aerosol direct and indirect effects, two-way WRF-
36 CMAQ shows improved performance over offline-coupled WRF and CMAQ in terms of
37 spatiotemporal distributions and statistics, especially for radiation, cloud forcing, O₃, sulfate,
38 nitrate, ammonium, and elemental carbon as well as tropospheric O₃ residual and column
39 nitrogen dioxide (NO₂). For example, the mean biases have been reduced by more than 10 W m⁻²
40 for shortwave radiation and cloud radiative forcing and by more than 2 ppb for max 8-h O₃.
41 However, relatively large biases still exist for cloud predictions, some PM_{2.5} species, and PM₁₀,
42 which warrant follow-up studies to better understand those issues. The impacts of chemistry-

43 meteorological feedbacks are found to play important roles in affecting regional air quality in the
44 U.S. by reducing domain-average concentrations of carbon monoxide (CO), O₃, nitrogen oxide
45 (NO_x), volatile organic compounds (VOCs), and PM_{2.5} by 3.1% (up to 27.8%), 4.2% (up to
46 16.2%), 6.6% (up to 50.9%), 5.8% (up to 46.6%), and 8.6% (up to 49.1%), respectively, mainly
47 due to reduced radiation, temperature, and wind speed. The overall performance of the two-way
48 coupled WRF-CMAQ model achieved in this work is generally good or satisfactory and the
49 improved performance for two-way coupled WRF-CMAQ should be considered along with other
50 factors in developing future model applications to inform policy making.

51 **Keywords:** CMAQ, Two-way coupling, Evaluation, Chemistry-meteorology feedback

52 **1. Introduction**

53 The Community Multiscale Air Quality (CMAQ) modeling system developed by the U.S.
54 Environmental Protection Agency (EPA) (Byun and Schere, 2006; Scheffe et al., 2016; San
55 Joaquin Valley APCD, 2018; Pye et al., 2020; U.S. EPA, 2020) has been extensively used by
56 both scientific community and governmental agencies over various geographical regions and
57 under different meteorological and air pollution conditions to address major key air quality
58 issues such as atmospheric ozone (O₃), acid rain, regional haze, and trans-boundary or long-
59 range transport of air pollutants during the past decades over North America (Zhang et al.,
60 2009a,b; Wang and Zhang, 2012; Hogrefe et al., 2015), Asia (Wang et al., 2009, 2012; Liu et al.,
61 2010; Zheng et al., 2015; Li et al., 2017; Xing et al., 2017; Yu et al., 2018; Mehmood et al.,
62 2020), and Europe (Kukkonen et al., 2012; Mathur et al., 2017; Solazzo et al., 2017). The
63 CMAQ model is traditionally driven offline by the three-dimensional meteorology fields
64 generated separately from other meteorological models such as the Weather Research and
65 Forecasting (WRF) model, and the dynamic feedbacks of chemistry predictions on meteorology

66 are neglected. However, more recently (IPCC, 2018), chemistry-meteorology feedbacks have
67 been found to play important roles in affecting the both global and regional climate change and
68 air quality (Jacobson et al., 1996; Mathur et al., 1998; Ghan et al., 2001; Zhang, 2008; Zhang et
69 al., 2010, 2015a,b, 2017; Grell and Baklanov, 2011; Wong et al., 2012; Baklanov et al., 2014; Yu
70 et al., 2014; Gan et al., 2015a; Wang et al., 2015a; Xing et al., 2015a,b; Yahya et al., 2015a,b;
71 Hong et al., 2017; Jung et al., 2019). Feedbacks of aerosols on radiative transfer through aerosol-
72 radiation interactions (i.e., aerosol direct forcing) and aerosol-cloud interactions (i.e., aerosol
73 indirect forcing) are especially important (Zhang, 2008; Zhang et al., 2015a,b; Baklanov et al.,
74 2014; Wang et al., 2015a; Yahya et al., 2015a,b). Recognizing this importance, as well as the
75 recent advances in knowledge on chemistry-meteorology interactions and computational
76 resources, the U.S. EPA developed a two-way coupled WRF-CMAQ model that accounts for the
77 aerosol direct effect alone (Wong et al., 2012). This version of CMAQ has been applied for both
78 regional and hemispheric studies (Wang et al., 2014; Hogrefe et al., 2015; Xing et al., 2016,
79 2017; Hong et al., 2017, 2020; Sekiguchi et al., 2018; Yoo et al., 2019). For example, Xing et al.
80 (2016) showed that aerosol direct feedbacks may further improve air quality resulting from
81 emission controls in the U.S. and also indicated that coupled models are key tools for quantifying
82 such feedbacks. Reduction in atmospheric ventilation resulting from aerosol induced surface
83 cooling can exacerbate ground level air pollution. Hong et al. (2017) estimated an increase by
84 4.8%-9.5% in concentrations of major air pollutants over China in winter due to incorporation of
85 such effects. Xing et al. (2017) reported that the aerosol direct effects could reduce daily max 1h
86 O₃ by up to 39 μg m⁻³ over China in January through reducing solar radiation and photolysis
87 rates. Hong et al. (2020) found that the benefits of reduced pollutant emissions through
88 weakening aerosol direct effects can largely offset the additional deaths caused by the warming

89 effect of greenhouse gases over China. Some of those studies have also found that the missing
90 aerosol indirect effects in WRF-CMAQ may introduce large model biases on their simulations of
91 radiation and thus air quality (Wang et al., 2014; Sekiguchi et al., 2018; Yoo et al., 2019). There
92 has been a growing awareness that both aerosol effects should be considered together to provide
93 greater fidelity in coupling complex atmospheric processes among chemistry, aerosols, cloud,
94 radiation, and precipitation (Grell and Baklanov, 2011). To address this issue and better represent
95 the one-atmosphere modeling capability of CMAQ, Yu et al. (2014) further extended the two-
96 way coupled WRF-CMAQ model by including aerosol indirect effects and improved WRF-
97 CMAQ's capability for predicting cloud and radiation variables.

98 Different from the traditional online integrated air quality models such as the Gas,
99 Aerosol, Transport, Radiation, General Circulation, and Mesoscale Meteorological (GATOR-
100 GCMM) model (Jacobson, 2001), the WRF model coupled with chemistry (WRF/Chem; Grell et
101 al., 2005) and the WRF model coupled with the Community Atmosphere Model version 5
102 (WRF-CAM5; Ma et al., 2013; Zhang et al., 2015a,b; 2017), in which atmospheric dynamics and
103 chemistry are integrated and simulated altogether without an interface between meteorology and
104 atmospheric chemistry (Zhang et al., 2013), two-way WRF-CMAQ (also referred to as the online
105 access model) is created by combining existing meteorology (i.e., WRF) and atmospheric
106 chemistry (i.e., CMAQ) models with an interactive interface (Yu et al., 2014). As pointed out by
107 Yu et al. (2014), the main advantage of two-way CMAQ is to allow the existing numerical
108 techniques to be used in both WRF and CMAQ to facilitate future independent development of
109 both models while also maintaining CMAQ as a stand-alone model (the offline capability). In the
110 past, a number of studies have compared and evaluated online vs. offline-coupled model
111 performance (Pleim et al, 2008; Matsui et al., 2009; Wilczak et al., 2009; Lin et al., 2010;

112 Herwehe et al., 2011; Yu et al., 2011; Wong et al., 2012; Zhang et al., 2013, 2016a; Choi et al.,
113 2019). However due to the missing offline-coupled mode or component for most online-coupled
114 models, many of those intercomparison studies are subject to some key limitations such as
115 inconsistent model treatments in chemical options (Matsui et al., 2009; Lin et al., 2010; Zhang et
116 al., 2013; Choi et al., 2019) or in both physical and chemical options (Wilczak et al., 2009;
117 Herwehe et al., 2011; Zhang et al., 2016a), different domain projection methods or resolutions
118 (Wilczak et al., 2009; Lin et al., 2010; Zhang et al., 2013), or disunified model inputs (Wilczak et
119 al., 2009; Lin et al., 2010; Zhang et al., 2013). Due to the unique coupling approach, two-way
120 WRF-CMAQ can be used to overcome those limitations and set up ideal intercomparisons
121 between online and offline simulations using consistent model treatments (Pleim et al, 2008; Yu
122 et al., 2011; Wong et al., 2012).

123 In this study, we provide a robust examination of model improvements by considering
124 chemistry-meteorology feedbacks and their impacts on the U.S. air quality using the two-way
125 WRF-CMAQ model (same version as in Yu et al., 2014) with both aerosol direct and indirect
126 effects. Long-term (five-year of 2008-2012) simulations using both two-way and offline coupled
127 WRF and CMAQ models are carried out and compared to the best of our knowledge for the first
128 time over the contiguous U.S. (CONUS) with anthropogenic emissions based on multiple years
129 of the U.S. National Emission Inventory (NEI) and chemical initial and boundary conditions
130 (ICONS/BCONS) downscaled from the advanced Earth system model, i.e., an updated version of
131 the Community Earth System Model/CAM5 (CESM/CAM5; He and Zhang, 2014; Glotfelty et
132 al., 2017). Our objectives include 1) perform a comprehensive model evaluation for major
133 meteorological variables and chemical species from this long-term application of the two-way

134 coupled WRF-CMAQ; and 2) conduct a comparative study of two-way and offline coupled WRF
135 and CMAQ to examine the impacts of chemistry-meteorology interactions on U.S. air quality.

136 Compared to previous studies in the literature, there are a few key features of this work.
137 First, the intercomparisons between two-way (or online) and offline WRF-CMAQ are performed
138 here using consistent model configurations including both physical/chemical options and inputs.
139 Second, unlike a few previous intercomparison studies (Pleim et al, 2008; Yu et al., 2011; Wong
140 et al., 2012) using two-way WRF-CMAQ with only aerosol direct effects for relatively short
141 episodes, the model version in this work includes both aerosol direct and indirect effects and
142 simulations are conducted for multiple years to provide more robust assessments. Third,
143 compared to other studies (e.g., Yahya et al., 2015a,b; Choi et al., 2019) focusing on the impacts
144 of chemistry-meteorology feedbacks on meteorology only or limited chemical species, this study
145 performs comprehensive and extensive evaluation and comparison to demonstrate importance of
146 chemistry-meteorology feedbacks on regional meteorology and air quality.

147 **2. Model description, simulation setup, and evaluation protocols**

148 Two sets of five-year (i.e., 2008-2012) long-term simulations are conducted using the two-
149 way coupled WRF v3.4-CMAQ v5.0.2 model with both aerosol direct and indirect effects and
150 the sequentially offline-coupled WRF v3.4 and CMAQ v5.0.2 model, respectively, over the
151 CONUS with 36-km horizontal grid spacing. The vertical resolution for these simulations
152 consists of 34 layers from the surface (~38 m) to 100 hPa (~15 km). The two-way coupled WRF-
153 CMAQ includes estimations of aerosol optical properties based on prognostic aerosol size
154 distributions and composition. These aerosol optical properties are then used to modulate the
155 shortwave radiation budget estimated using the Rapid and accurate Radiative Transfer Model for

156 General circulation (RRTMG) radiation scheme (Iacono et al., 2008) in WRF. Additionally,
157 aerosol indirect effects, including the first (cloud albedo) and second (cloud lifetime) indirect
158 aerosol forcing and the glaciation (ice and mixed-phase cloud lifetime) indirect aerosol forcing
159 are also modeled. More details on the model development of this version of WRF-CMAQ can be
160 found in Yu et al. (2014). On the other hand, the WRF only model calculates the radiation
161 budgets by using prescribed aerosol optical properties such as aerosol optical depth, single
162 scattering albedo and asymmetry parameters and cloud formation by assuming default droplet
163 number concentration and fixed cloud effective radius, which may not be representative for the
164 large regions with complex air pollution conditions. Both the two-way and offline coupled WRF-
165 CMAQ use the same model configurations as shown in Table S1 in the supplementary material,
166 except that prognostic aerosol impacts on radiation and clouds are fully treated in two-way
167 WRF-CMAQ. The physics options include the RRTMG shortwave and longwave radiation
168 schemes, the Asymmetric Convective Model (ACM2) planetary boundary layer (PBL) scheme
169 (Pleim, 2007), the Pleim-Xiu (PX) land-surface scheme (Xiu and Pleim, 2001), the Morrison
170 two-moment microphysics scheme (Morrison et al., 2009), and version 2 of the Kain-Fritsch
171 (KF2) cumulus scheme (Kain, 2004). The chemical options include the Carbon Bond 2005
172 (CB05) chemical mechanism (Yarwood et al., 2005) with additional chloride chemistry (Sarwar
173 et al., 2008), the sixth generation CMAQ aerosol module (AERO6) (Appel et al., 2013), and
174 CMAQ's aqueous phase chemistry (AQCHEM). In addition, the time steps of dynamics and
175 radiation for two-way WRF-CMAQ are set as 1 min and 15 mins, respectively, and the call
176 frequency for CMAQ in the two-way coupled model is set to be 5 mins.

177 The meteorological ICONS/BCONs are generated from the National Centers for
178 Environmental Prediction Final Analysis (NCEP-FNL) datasets and the chemical

179 ICONs/BCONs are downscaled from a modified version of CESMv1.2.2/CAM5 (He and Zhang,
180 2014; Glotfelty et al., 2017). The chemical ICONs/BCONs generated from CESM simulations
181 consider the year-to-year variation. The CESM simulations have been comprehensively
182 evaluated against surface, remote sensing including satellite data, and reanalysis data for major
183 meteorological and chemical variables over Europe, Asia, North America, and the globe. The
184 results are also compared with other existing global model results and show generally
185 satisfactory/superior performance. The anthropogenic emissions are based on two versions of
186 NEI. NEI 2008 and NEI 2011 are used to cover the 5-year period, i.e., NEI 2008 for 2008-2010
187 and NEI 2011 for 2011-2012, respectively. Biogenic emissions are calculated online using the
188 Biogenic Emissions Inventory System (BEIS) v3 (Schwede et al., 2005). The sea-salt and dust
189 emissions are also generated online by CMAQ's inline modules (Zender et al., 2003; Zhang et
190 al., 2005; Foroutan et al., 2017). Two-way coupled WRF-CMAQ simulations are reinitialized
191 every 5 days for meteorology fields only. We have conducted sensitivity simulations in the past
192 (Wang et al., 2021) and found that a 5-day reinitialization frequency is more suitable to improve
193 the overall simulation quality to make meteorology simulations as accurate as possible while
194 preserving the two-way chemistry-meteorology feedbacks. The WRF-only simulations that are
195 used to drive the offline CMAQ simulations apply the same reinitialization method to make sure
196 any deviation between two simulations are more determined by the feedback processes
197 consistent with the two-way coupled WRF-CMAQ simulations.

198 The model evaluation in this work mainly focuses on the long-term climatological type of
199 performance in representative seasons (i.e., winter and summer) by comparing 5-year average
200 spatially and temporally matched model predictions of major surface meteorological/radiation-
201 cloud variables and surface/column chemical species against various surface/satellite

202 observations and reanalysis data [\(The 5-year annual results can be found in the supplemental](#)
203 [materials\)](#). [A brief inter-annual comparison between observations and two-way CMAQ](#)
204 [simulations are also performed for selected major meteorological and chemical variables to](#)
205 [examine the model's capability in reproducing the year-to-year variations of those variables.](#) The
206 surface meteorological data include temperature at 2 m (T2), relative humidity at 2 m (RH2),
207 wind speed at 10 m (WS10), and wind direction at 10 m (WD10) from the National Climatic
208 Data Center (NCDC), and precipitation from the NCDC, the National Acid Deposition Program
209 (NADP), the Global Precipitation Climatology Project (GPCP), the Parameter-elevation
210 Regressions on Independent Slopes Model (PRISM), and the Tropical Rainfall Measuring
211 Mission Multisatellite Precipitation Analysis (TMPA). The radiation and cloud data include
212 downward shortwave radiation at the ground surface (SWDOWN), net shortwave radiation at the
213 ground surface (GSW), downward longwave radiation at the ground surface (GLW), outgoing
214 longwave radiation at the top of the atmosphere (OLR), and shortwave and longwave cloud
215 forcing (SWCF and LWCF) from the Clouds and the Earth's Radiant Energy System (CERES);
216 aerosol optical depth (AOD), cloud fraction (CF), cloud water path (CWP), and cloud optical
217 thickness (COT) from the MODerate resolution Imaging Spectroradiometer (MODIS); and cloud
218 droplet number concentration (CDNC) derived based on MODIS data by Bennartz (2007). The
219 chemical data include surface O₃ from the Aerometric Information Retrieval System-Air Quality
220 Subsystem (AIRS-AQS) and the Clean Air Status and Trends Network (CASTNET); surface ~~fine~~
221 particulate matter [with 2.5 μm or less](#) (PM_{2.5}) and its constituents including sulfate (SO₄²⁻),
222 nitrate (NO₃⁻), ammonium (NH₄⁺), elemental carbon (EC), organic carbon (OC), and total carbon
223 (TC = EC + OC) from the Interagency Monitoring of Protected Visual Environments
224 (IMPROVE) and the Chemical Speciation Network (CSN); surface ~~coarse~~-particulate matter

Formatted: Font: Symbol

225 with diameters of 10 μm or less (PM₁₀) from the AQS; and column abundance variables such as
226 column carbon monoxide (CO) from the Measurements of Pollution in the Troposphere
227 (MOPITT), tropospheric ozone residual (TOR) from the Ozone Monitoring Instrument (OMI),
228 and column nitrogen dioxide (NO₂) and formaldehyde (HCHO) from the Scanning Imaging
229 Absorption Spectrometer for Atmospheric Chartography (SCIAMACHY).

Formatted: Font: Symbol

230 The satellite datasets used in this study are all level-3 gridded monthly-averaged data
231 with various resolutions (i.e., 0.25° for OMI and PRISM, 0.5° for SCIAMACHY, 1° for CERES,
232 GPCP, MODIS, and MOPITT). For the calculation of model performance statistics, the satellite
233 data with different resolutions are mapped to CMAQ's Lambert conformal conic projection
234 using bi-linear interpolation in the NCAR command language. CMAQ model outputs at
235 approximate time of the satellite overpass are paired with the satellite retrievals to facilitate a
236 consistent comparison. Note that only those grid points with valid satellite observations are
237 considered when paring model results with observations, and the averaging kernels are not
238 considered when analyzing the column CO and NO₂ results, which may introduce some
239 uncertainties (Wang et al., 2015b). Modeled CDNC is calculated as the average value of the
240 layer of low-level warm clouds between 950 and 850 hPa as suggested by Bennartz (2007).
241 Following the approach of Wielicki et al. (1996), the SWCF and LWCF are calculated as the
242 difference between the clear-sky and the all-sky reflected radiation at the top of atmosphere for
243 both simulations and observations.

Formatted: Subscript

244 The statistical performance evaluation follows a protocol similar to that of Zhang et al.
245 (2006, 2009a) and Yahya et al. (2016) and uses well-accepted statistical measures such as
246 correlation coefficient (R), mean bias (MB), root mean square error (RMSE), normalized mean
247 biases (NMB), and normalized mean error (NME) (S. Yu et al., 2006). Because of different

248 sampling protocols among monitoring networks, the evaluation is conducted separately for
249 individual networks for the same simulated variables/species.

250 3. Comprehensive model evaluation of two-way WRF-CMAQ

251 3.1 Meteorological evaluation

252 3.1.1 Surface meteorological variables

253 Figures 1a-d show the spatial distribution of 5-year average MBs for T2, RH2, WS10,
254 and hourly precipitation from two-way WRF-CMAQ against the NCDC data in winter and
255 summer, 2008-2012 and Tables 1 and 2 summarize the statistics for the same variables. ~~All~~
256 Most variables except for precipitation show overall moderate to good ~~or moderate~~ spatial
257 performance with many sites showing MBs within $\pm 1.00-6$ °C for T2, ± 105 % for RH2, ± 1 m s⁻¹
258 for WS10, and ± 0.24 mm hr⁻¹ for precipitation, respectively in both seasons. WRF-CMAQ tends
259 to overpredict T2 (i.e., warm bias) over widespread areas of domain especially along the Atlantic
260 coast, the eastern/southeastern U.S., the Central U.S., and Pacific coast in winter and
261 underpredict T2 (i.e., cold bias) over the eastern U.S., the Central U.S., and mountainous U.S. in
262 summer, which leads to an overall small warm bias in the whole year (see Figure S1). The model
263 also shows cold biases (i.e., underprediction in T2) over the mountainous regions and
264 northeastern U.S. Similar warm biases of T2 in winter have been previously reported by Cohen
265 et al. (2015) and are found to be associated with the relatively deeper PBL depth using the non-
266 local ACM2 PBL scheme. The relatively larger warm/cold biases over coastal and mountainous
267 areas are likely caused by due to the coarse spatial-grid spacing of 36-km ~~which that~~ cannot well
268 resolve the complex topography (Yahya et al., 2016). Compared to many previous WRF studies
269 (Wang et al., 2012; Brunner et al., 2015; Yahya et al., 2016), which typically show cold T2

270 biases, the overall small warm biases in this study can be attributed to the soil moisture nudging
271 technique used in the PX land surface scheme (Pleim and Gilliam, 2009). The spatial patterns of
272 MBs for RH2 show a ~~clear-general~~ anti-correlation compared to T2 (i.e., RH2 is overpredicted
273 where T2 is underpredicted and vice versa) ~~due to the way how RH2 is calculated based on T2-~~
274 ~~This is consistent with how RH2 is calculated based on T2.~~ The spatial distribution of MBs for
275 WS10 also shows dominant overpredictions ~~in both winter and summer~~ especially along
276 coastlines, indicating the prescribed sea-surface temperature might not be sufficient to resolve
277 the air-sea interactions. Systematic overpredictions of hourly precipitation against NCDC data ~~in~~
278 ~~both seasons~~ are found to be mainly caused ~~by~~ low non-convective precipitation events and
279 ~~should-can~~ be attributed to ~~the uncertainties associated with~~ the Morrison microphysics scheme
280 (Yahya et al., 2016).

281 The precipitation performance is further examined by comparing WRF-CMAQ with
282 ~~GPCP-TMPA~~ and PRISM as shown in Figures ~~1e-g2~~. The spatial distribution of precipitation is
283 well simulated by WRF-CMAQ especially over the ~~land~~CONUS against ~~both GPCP and~~
284 ~~PRISM observations~~ by capturing the hot spots along the Pacific Northwest coast ~~in winter~~ and
285 some areas over ~~eastern the Central U.S. and FL in summer~~. Moderate overpredictions of
286 precipitation against ~~GPCP-TMPA~~ over the Atlantic Ocean and Gulf of Mexico ~~in summer~~ are
287 also evident, possibly ~~due to caused by~~ overprediction of convective precipitation ~~intensity~~ by the
288 Kain-Fritsch ~~emulus~~ scheme (Hong et al., 2017) over ocean. As shown in Tables 1 ~~and 2~~, the
289 domain-average ~~seasonal~~ statistics demonstrate good performance for all variables except for
290 precipitation against NCDC in terms of MBs, NMBs, RMSE, and Rs. For example, the MBs for
291 T2, RH2, WS10, and precipitation are ~~10.1 °C, 2.2%, 0.5744 m s⁻¹, and 0.0514-0.2328 mm day⁻¹~~
292 ~~(except for 0.71 mm day⁻¹ for NCDC) in winter and -1.1 °C, 3.7%, 0.38 m s⁻¹, and 0.13-0.23 mm~~

Formatted: Superscript

293 day⁻¹ (except for 0.75 mm day⁻¹ for NCDC) in summer, respectively, and Rs for those variables
294 are typically between 0.5-0.978, which are well within the performance benchmark values
295 recommended by Zhang et al. (2013) and Emery et al. (2017).

296 Figure 3 shows the bar charts of annual trends for T2, RH2, WS10, and precipitation in
297 2008-2012. Two-way WRF-CMAQ predicts the annual average T2 very well with MBs <
298 0.25 °C in all years. The simulation can also capture the increasing trend of T2 from 2008 to
299 2012 observed by NCDC. RH2 is consistently overpredicted by the two-way WRF-CMAQ in all
300 years despite relatively low biases (MBs < 3%). Both observations and simulations show the
301 lowest RH2 in 2012 and the highest in 2009. As also shown in Figure 1, the model tends to
302 systematically overpredict both WS10 and precipitation throughout all years as well. There are
303 no clear trends (i.e., increasing or decreasing) for WS10 and precipitation between 2008 to 2012
304 from either observations or simulations. However two-way WRF-CMAQ is able to capture both
305 the lowest wind speed and precipitation in 2012 and the highest wind speed in 2008 from
306 observations. In general, the model performs very well in reproducing the year-to-year variation
307 for the major meteorological variables between 2008 to 2012.

308 **3.1.2 Radiation and cloud variables**

309 Figures 4 and 52 compares the 5-year average spatial distribution of major radiation
310 variables (i.e., SWDOWN, GSW, GLW, OLR, and AOD) based on the satellite retrievals and
311 two-way WRF-CMAQ simulations in winter and summer, 2008-2012, and Tables 1 and 2
312 summarizes the domain-average model performance statistics. WRF-CMAQ predicts the
313 longwave radiation variables GLW and OLR very well with domain-average of NMBs of -
314 0.34-9% and 10.8% in winter and -3.6% and 0.9% in summer, respectively, and Rs of 0.96 to

315 0.99 for both. The shortwave radiation variables SWDOWN and GSW are slightly overpredicted
316 on average with NMBs of 113.39% and 7.5444% in winter and 17.1% and 15.1% in summer,
317 respectively, and Rs of ranging from 0.75 to 0.997 for both. The simulations also reliably
318 reproduce the spatial distribution of both longwave and shortwave radiation compared to
319 observations in both seasons. The relatively large overpredictions for shortwave radiation
320 especially in summer are very likely caused by the large underpredictions of aerosol direct
321 radiative forcing reflected from the underpredictions of AOD (Figure 52) as well as
322 underprediction of indirect cloud radiative forcing (see Figure 83). It has been reported that WRF
323 v3.4 does not treat the subgrid cloud feedback to radiation, which could also contribute to the
324 overpredictions in shortwave radiation especially in summer (Alapaty et al., 2012; Hong et al.,
325 2017). The model largely underpredicts the magnitude of AOD in both seasons (NMBs of: -64.8
326 -59.8% in winter and -67.8% in summer), while providing a reasonable representation of the
327 spatial distribution of AOD over the U.S., with generally higher values over the Midwest in
328 winter and over the eastern U.S. in summer and lower values in the west. The model also
329 underpredicts the elevated AODs over oceans and the northern part of domain in both seasons.
330 Similar AOD underpredictions have been reported in previous studies over the U.S. using two-
331 way coupled WRF-CMAQ (Gan et al., 2015a; Hogrefe et al., 2015; Xing et al., 2015a). The
332 relatively large underpredictions of AOD may be caused by several factors. First,
333 underprediction of PM_{2.5} concentrations, particularly SO₄²⁻ in both seasons and OC in summer
334 (Tables 3 and 42), can contribute significantly to the underprediction of AOD, especially over
335 the eastern U.S. Second, the underestimation of dust emissions may contribute to missing hot
336 spots from the model over arid areas in CA and AZ (Foroutan et al., 2017 Zender et al., 2003) and
337 underestimates of sea-salt emissions may lead to missing elevated AODs over oceans (Gan et al.,

338 2015b). Third, challenges in adequately representing prescribed and wildfire emissions in the
339 NEI (Kelly et al., 2019) may cause many missing hot spots over large areas of the Pacific
340 Northwest, CA, Canada, and the eastern U.S. especially in summer. Fourth, uncertainties in
341 BCONs of PM_{2.5} concentrations may further contribute to underpredictions of AOD over oceans
342 and the northern part of the domain. For example, Kaufman et al. (2001) found that the
343 background AOD could reach 0.1 over the Pacific Northwest using Aerosol Robotic Network
344 (AERONET) data. The AODs in the current simulation seem to be biased low (between 0.026-
345 0.068 in both seasons over the Pacific Ocean) and indicate potential underpredictions of PM_{2.5}
346 BCONs, especially in the free troposphere. Finally, there are uncertainties associated with
347 MODIS retrievals. Remer et al. (2005) found that the uncertainty of level 3 MODIS monthly
348 AODs can be up to $\pm 0.05 \pm 0.15$ AOD over the land due to clouds and surface reflectance. More
349 AOD data from other satellites or AERONET might be considered in the future work to provide
350 more robust ensemble type of evaluation for AOD.

351 Figures ~~6-83 and 4~~ compare the 5-year average spatial distribution of major cloud and
352 cloud radiative variables for the satellite retrievals and two-way WRF-CMAQ simulations in
353 winter and summer, 2008-2012, and Tables 1 and 2 summarizes the ~~domain-average model~~
354 ~~performance~~ corresponding statistics. As shown in Figures 6 and 73, WRF-CMAQ tends to
355 largely underpredict CDNC, COT, and CWP in both seasons over most of the ~~whole~~ domain
356 with the domain-average NMBs of -82.44%, -80.81%, and ~~-45.43%~~ in winter and -79.2%, -
357 83.6%, and -66.3% in summer, respectively. Despite the large underprediction of those cloud
358 variables, the spatial correlations are generally predicted well, especially for COT and CWP with
359 Rs ranging from 0.63 to 0.74 of 0.84 and 0.79, respectively. Compared to the other cloud
360 variables, CF is much better predicted with an NMB of -10.42% and an R of 0.8792 in winter

361 and an NMB of -23.0% and an R of 0.81 in summer, respectively, which is consistent with the
362 performance reported in Yu et al. (2014). The model can reproduce the high CFs over northern
363 and northeastern part of domain as well as over oceans while capturing the low CFs over the
364 mountainous and plateau regions in the U.S. and Mexico especially in winter. In addition to the
365 underprediction of PM_{2.5} (thus underestimating CCN), the large underpredictions of cloud
366 variables (especially CDNC and COT) can be attributed to uncertainties in aerosol microphysics
367 schemes (Yahya et al., 2016) as well as missing aerosol indirect effects on subgrid convective
368 clouds (Yu et al., 2014). Gantt et al. (2014) and Zhang et al. (2015b) also showed the aerosol
369 activation scheme (i.e., Abdul-Razzak and Ghan, 2000) used in the current version of WRF-
370 CMAQ may have underestimated CDNC and thus CWP and COT due to some missing processes
371 such as insoluble aerosol adsorption and giant cloud condensation nuclei. Overall, the relatively
372 poor model performance for cloud variables reflects current limitations in representing aerosol
373 indirect effects and aerosol-cloud interactions in state-of-science online coupled models. Further
374 model improvements that incorporate new knowledge from emerging studies should be
375 conducted in the future.

376 As shown in Figure 84, WRF-CMAQ predictions of SWCF and LWCF generally agree
377 well with the satellite observations in both seasons-based values. The model partially-can
378 captures the elevated SWCF and LWCF over the Atlantic Ocean, Pacific Northwest, and
379 widespread areas over the eastern U.S. in winter and those over the Pacific Northwest, northern
380 part of the domain, and Atlantic Ocean in summer. The domain-average NMBs are -11.126.0%
381 for SWCF and -15.122.2% for LWCF in winter and -41.3% for SWCF and -33.3% for LWCF in
382 summer, respectively. The relatively larger biases in summer compared to winter are correlated
383 with larger biases associated with radiation and cloud predictions potentially caused by larger

384 [underpredictions of aerosol predictions](#). As discussed earlier, the underpredictions of SWCF may
385 partially contribute the overprediction of SWDOWN (more shortwave radiation reaching the
386 ground) and those of LWCF may further lead to the overpredictions in OLR (more longwave
387 radiation emitted into the space). The performance of SWCF and LWCF is consistent with the
388 12-km simulation reported in Yu et al. (2014) and even slightly better in terms of NMBs, which
389 might be associated with the long-term vs. short-term simulations. It is also worth noting that
390 SWCF (LWCF) is calculated as the difference between the clear-sky and all-sky shortwave
391 (longwave) radiation at the top of atmosphere, and so performance for SWCF and LWCF
392 depends on performance for both radiation and cloud properties. The generally better
393 performance in terms of model bias for SWCF and LWCF compared to the cloud variables
394 seems to be driven by the relatively good performance of shortwave/longwave radiation in the
395 model.

396 **3.2 Chemical evaluation**

397 **3.2.1 O₃**

398 Figure [95a](#) shows the spatial distribution of simulated average daily maximum 8-h O₃ [in](#)
399 [summer, 2008-2012](#) from two-way WRF-CMAQ overlaid with observations from both the
400 AIRS-AQS and CASTNET networks. WRF-CMAQ shows good performance by capturing the
401 spatial distribution of max 8-h O₃ over widespread areas of the domain. The model tends to
402 overpredict O₃ along coastlines in the southeastern U.S., Gulf of Mexico, and Pacific coast,
403 which can be attributed to a poor representation of coastal boundary layers (Yu et al., 2007); ~~the~~
404 ~~warm T2 biases as shown in Figure 1,~~ and lack of O₃ sink via halogen chemistry (Sarwar et al.,
405 2015) and deposition to water (Gantt et al., 2017). The simulation also underpredicts O₃ in

406 widespread areas in the Midwest, ~~eastern~~Central, and mountainous regions of the U.S., which is
407 consistent with the results of 36-km simulations from Wang and Zhang (2012) that used an
408 earlier version of CMAQ v4.6 with the same CB05 gas-phase mechanism. In addition to cold T2
409 biases over those areas (Figure 1), the underpredictions are also believed to be associated with
410 inaccurate representations of precursor emissions and elevated/complex terrain due to the coarse
411 grid spacing of 36-km over those regions. Wang and Zhang (2012) found that their 12-km
412 simulation showed improved performance over similar regions especially in summer.

413 Figure 95c shows the monthly variation of domain-average 5-year average O₃ mixing
414 ratios between observations from AIRS-AQS and simulations from two-way WRF-CMAQ, and
415 Figure 95d shows the diurnal variation of domain-average 5-year average hourly O₃ mixing
416 ratios between observations from CASTNET and simulations from two-way WRF-CMAQ for
417 ~~representative winter (DJF and blue color) and summer (JJA and red color) seasons~~. As shown in
418 Figure 95c, the O₃ mixing ratios are overpredicted throughout the year, which is consistent with
419 overprediction of T2 (figure not shown). The largest overprediction occurs in the relatively cold
420 months such as September to December. It is interesting that the observations show the largest
421 monthly O₃ mixing ratios in spring and early summer while the simulation shows the peak
422 during the summer. The difference in timing of peak O₃ between observations and simulations
423 during the year might be associated with uncertainties in the BCONs of O₃ that reflect impacts of
424 the long-range transport and associated stratosphere-troposphere exchange of O₃. As shown in
425 Figure 95d, WRF-CMAQ tends to overpredict O₃ during most hours (i.e., 2:00-18:00) in summer
426 and throughout the whole day in winter partially due to the overprediction of T2, especially in
427 winter (~~figure not shown~~Figure 1). The diurnal pattern of O₃ is captured much better during
428 summer with much less prediction bias, especially during the nighttime, indicating that the

429 model does a better job in predicting the evolution of nocturnal boundary layer and atmospheric
430 chemistry in the warm season than the cold season. The overall overpredictions in this work are
431 also consistent with previous studies (Eder and Yu, 2006; Appel et al., 2007; Wang et al., 2012),
432 although our results show much better nighttime performance owing to the application of the
433 ACM2 scheme that treats both local and non-local closure (Pleim, 2007). As also shown in Table
434 42, the domain-average NMBs and NMEs for max 8-h O₃ in summer are 10.62-6% and 13.24%
435 against AQS and -3.04-5% and 11.58-4% against CASTNET, respectively. The statistics
436 are also consistent with previous studies using the CMAQ model (Zhang et al., 2009a; Appel et
437 al., 2013, 2017; Penrod et al., 2014) and can be considered as good performance according to the
438 criteria suggested by Zhang et al. (2013) and Emery et al. (2017).

439 Figure 3 also shows the bar charts of annual trends for max 8-h O₃ from two-way WRF-
440 CMAQ against AQS and CASTNET observations in 2008-2012. Two-way WRF-CMAQ
441 systematically overpredicts O₃ especially against AQS data with MBs typically > 4.0 ppb. The
442 potential reasons for model biases have been discussed earlier in this section. There are no
443 obvious decreasing or increasing trends for max 8-h O₃ from AQS or CASTNET observations.
444 However, the model can generally capture the high O₃ mixing ratios in 2008 and 2010 and the
445 low O₃ mixing ratios in 2009 from both AQS and CASTNET. The similar down and up trends
446 between 2008 to 2010 for O₃ (i.e., decreasing from 2008 to 2009 and increasing from 2009 to
447 2010) from AQS observations were also found by Yahya et al. (2016), but not captured by their
448 simulations. Zhang and Wang (2016) was able to reproduce the similar trend over the
449 southeastern U.S. between 2008 to 2010 using their models and attributed the abnormal high
450 2010 O₃ mixing ratios to the extreme dry and warm weather conditions during fall 2010.

451 3.2.2 Aerosols

Formatted: Subscript

Formatted: Subscript

Formatted: Subscript

Formatted: Subscript

Formatted: Subscript

Formatted: Subscript

Formatted: Subscript

452 Figures 106a and 10c shows the spatial distribution of simulated 5-year average PM_{2.5}
453 from two-way WRF-CMAQ overlaid with observations from both the CSN and IMPROVE
454 networks in winter and summer, 2008-2012 and Figure S1 shows the spatial distribution of the
455 major PM_{2.5} constituents overlaid with observations from the CSN and IMPROVE network and
456 PM_{1.0} overlaid with observations from the AQS network. As shown, WRF-CMAQ performs well
457 for PM_{2.5} over widespread areas of the Midwest and northeastern U.S. in both seasons, while
458 PM_{2.5} is underpredicted over the southeastern and western U.S. especially in winter. The model
459 also misses some hot spots of observed concentrations in the western U.S., which are mainly
460 caused by TC underpredictions (Figure S64) that are likely linked to poorly allocated and
461 underestimated wildfire emissions in the NEI (Wiedinmyer et al., 2006; Roy et al., 2007; Kelly
462 et al., 2019). The relatively large underpredictions over the eastern U.S. are mainly caused by the
463 combined effects from SO₄²⁻, NH₄⁺, and TC. As shown in Figure S64, WRF-CMAQ largely
464 underpredicts SO₄²⁻ in the Midwest and southeastern U.S. mainly due to the underprediction of
465 oxidants such as O₃ (see Figure 95a) (which leads to less production from the gaseous oxidation),
466 overprediction of precipitation (see Figure 24d) (which leads to more wet deposition and
467 removal), and large underprediction of cloud fields (see Figures 6-73) (which leads to less
468 aqueous phase formation), over the same area. On the other hand, NH₄⁺ and NO₃⁻ are either
469 underpredicted or overpredicted, respectively, over the similar areas mainly due to
470 underprediction of SO₄²⁻. According to the aerosol thermodynamics, when SO₄²⁻ is
471 underpredicted, NH₄⁺ tends to be underpredicted due to its major role as cation. More gaseous
472 NH₃ will be available to neutralize NO₃⁻, thus leading to overprediction of NO₃⁻ especially over
473 the sulfate poor regions (West et al., 1999). Other potential reasons include the inaccurate
474 assumptions in the thermodynamic module (for example, the internally mixed aerosol state and

475 equilibrium assumption may not be representative over some regions and different time periods,
476 S. Yu et al., 2006), uncertainties in emissions of key species such as NH₃ and non-volatile
477 cations that affect particle acidity (Mebust et al., 2003; Wang and Zhang, 2014; Vasilakos et al.,
478 2018; Pye et al., 2020), and measurement errors especially for NO₃⁻ and NH₄⁺ (X.-Y. Yu et al.,
479 2006; Karydis et al., 2007; Wang and Zhang, 2012). TC underpredictions over most sites of the
480 domain can be attributed to the underprediction of emissions (e.g., wildfire and primary OC) and
481 underestimation of secondary organic aerosol (SOA) formation (Appel et al., 2017; Pye et al.,
482 2017) since EC (a chemically inert species) is overpredicted, which suggest that atmospheric
483 mixing did not drive the TC underpredictions.

484 ~~Figures 6e-6h show the scatter plots of major PM_{2.5} components such as SO₄²⁻, NH₄⁺, and~~
485 ~~NO₃⁻ and TC. The WRF-CMAQ predicts PM_{2.5} constituents well with the majority of data~~
486 ~~within the 1:2 ratio lines. Systematic underpredictions of SO₄²⁻ and NH₄⁺ and overpredictions of~~
487 ~~NO₃⁻ are shown, which are consistent with their spatial distributions. Relatively large under- and~~
488 ~~overpredictions of TC compensate each other and lead to relatively low overall model biases. As~~
489 ~~also shown in Figure S1, the model fails to reproduce high concentrations of PM₁₀ (those > 20~~
490 ~~µg m⁻³) over widespread areas of the domain, especially over dust source areas in CA, AZ, and~~
491 ~~NM. Hong et al. (2017) found the similar large underprediction of dust using CMAQ v5.0.2 over~~
492 ~~China and attributed it to a too high threshold for friction velocity in the current dust module~~
493 ~~(Dong et al., 2016). Sea salt also seems to be underpredicted by WRF-CMAQ, although sea salt~~
494 ~~predictions are better than dust as shown along the coastlines.~~

495 Figures 1066e and 10f6d show the monthly variation of 5-year average PM_{2.5} between
496 observations from CSN and IMPROVE, respectively, and simulations from two-way WRF-
497 CMAQ. Both observations and WRF-CMAQ show higher monthly-PM_{2.5} concentrations at CSN

498 ~~sites~~ than IMPROVE ~~sites throughout for~~ the whole year because most of CSN sites are in more
499 polluted urban areas while majority of IMPROVE sites are in rural areas and national parks. The
500 model tends to underpredict PM_{2.5} over both CSN and IMPROVE sites in the warm months (i.e.,
501 April to September) mainly due to the underpredictions of SO₄²⁻ and OC while it overpredicts
502 PM_{2.5} in cold months mainly due to NO₃⁻. The model also captures the seasonality of PM_{2.5}
503 better over CSN sites than IMPROVE sites, especially in the summer months. The large
504 underpredictions over IMPROVE sites during summer months are likely due to the
505 underestimation of precursor emissions (such as wildfire emissions).

506 Figure 11 shows the scatter plots of major PM_{2.5} components such as SO₄²⁻, NH₄⁺, and
507 NO₃⁻, and TC in winter and summer, 2008-2012. The WRF-CMAQ predicts PM_{2.5} constituents
508 well with majority of data within the 1:2 ratio lines in both seasons. Systematic underpredictions
509 of SO₄²⁻ and NH₄⁺ in winter and overpredictions of NO₃⁻ in summer are shown, which are
510 consistent with their spatial distributions. Relatively large under- and overpredictions of TC
511 especially in winter compensate each other and lead to relatively low overall model biases. As
512 also shown in Figure S6, the model fails to reproduce high concentrations of PM₁₀ (those > 20
513 µg m⁻³) over widespread areas of the domain, especially over dust source areas in CA, AZ, and
514 NM. Hong et al. (2017) found the similar large underprediction of dust using CMAQ v5.0.2 over
515 China and attributed it to a too-high threshold for friction velocity in the current dust module
516 (Dong et al., 2016). Sea-salt also seems to be underpredicted by WRF-CMAQ, although sea-salt
517 predictions are better than dust as shown along the coastlines.

518 Figure 3 shows the bar charts of annual averaged observations and simulations for PM_{2.5}
519 over the CSN and IMPROVE sites. Overall, the model performs well for PM_{2.5} for most of years
520 and better over CSN than IMPROVE sites with general underpredictions in most years. The

Formatted: Subscript

Formatted: Subscript

521 observations for both CSN and IMPROVE show a general decreasing trend (except for 2010
522 over CSN) especially over IMPROVE sites. Two-way WRF-CMAQ is able to reproduce the
523 declining trend well particularly over IMPROVE sites and again demonstrate its capability in
524 accurately simulating the year-to-year variations of not only meteorology but air quality.

525 ~~There are no universally accepted performance criteria for aerosols.~~ As recommended by
526 some previous studies (Zhang et al., 2006; Wang and Zhang, 2012; Emery et al., 2017),
527 generally $\pm 15\%$ and $\pm 30\%$ for model biases and 30% and 50% for model errors can be
528 considered as good and acceptable performance. As shown in Tables 3 and 42, WRF-CMAQ in
529 this work demonstrates an overall good or acceptable performance in predicting aerosols in terms
530 of statistics especially for $PM_{2.5}$ in both seasons, NO_3^- , NH_4^+ , ~~OC~~, and TC in winter, and SO_4^{2-}
531 and NH_4^+ in summer. It shows the domain-average NMBs of -7.29% and ~~8.6-13.7%~~ in winter
532 ~~and -13.2% and -26.9% in summer~~ for $PM_{2.5}$ against CSN and IMPROVE, respectively; NMBs
533 of ~~-10.226.7%~~ and ~~-20.927.2%~~ in in summer for SO_4^{2-} against CSN and IMPROVE,
534 respectively; NMBs of ~~-0.346.6%~~ and ~~13.34.6%~~ in winter for NO_3^- against CSN and IMPROVE,
535 respectively; an NMB of ~~3-14.3%~~ for NH_4^+ in summer against CSN; ~~NMBs of 20.6% and 29.4%~~
536 ~~for EC against CSN and IMPROVE, respectively~~; an NMB of ~~13.0-28.9%~~ in winter for OC
537 against IMPROVE; and NMBs of ~~7.2-9.4%~~ and ~~17.5-9.2%~~ in winter for TC against CSN and
538 IMPROVE, respectively. The relatively large underpredictions of PM_{10} in both seasons, i.e., ~~an~~
539 NMBs of ~~-36.345.9%~~ in winter and -45.8% in summer against AQS, indicate further
540 improvements of dust emissions are warranted. Overall, the aerosol performance is also
541 comparable or better than previous CMAQ or WRF-CMAQ applications (Wang and Zhang,
542 2012; Penrod et al., 2014; Yu et al., 2014). For example, Penrod et al. (2014) showed 5-year
543 (2001-2005) ~~averagesummer-mean~~ NMBs of ~~-23.3% and 4.0% in winter and~~ -19.1% to -17.6%

Formatted: Subscript

Formatted: Superscript

544 [in summer](#) for PM_{2.5} against CSN and IMPROVE data over the CONUS using the CMAQ v5.0
545 and Yu et al. (2014) reported the monthly mean NMBs of -6.2% and -16.8% for PM_{2.5} against
546 CSN and IMPROVE over the eastern U.S. using the same version of WRF-CMAQ as that used
547 in this study.

548 3.2.3 Column abundance

549 Figures [12 and 137](#) shows the spatial distribution of 5-year average column abundances
550 between various satellite products and two-way WRF-CMAQ for column CO, TOR, column
551 NO₂, and column HCHO [in winter and summer, 2012](#); and Tables [3 and 42](#) summarizes the
552 statistics. As shown, WRF-CMAQ can reproduce the spatial distribution of the column
553 abundances of gases quite well [in both seasons except for column HCHO in winter](#) with Rs
554 ranging from 0.[7083](#) to 0.[8794](#). TOR [in both seasons](#), column NO₂ [in winter](#) and column HCHO
555 [in summer](#) are also generally well predicted in terms of magnitudes with NMBs of [4.74-6% for](#)
556 [TOR and; 0.3 for NO₂-14.5%, and 18.0%](#), respectively, [in winter and -8.0% for TOR and 15.0%](#)
557 [for HCHO, respectively, in summer](#). Systematic underpredictions for column CO occur [in both](#)
558 [seasons](#) over the whole domain with ~~an~~-NMBs of [-20.56-6% in winter and -27.8% in summer](#) for
559 a few reasons. First, the BCONs of CO may be significantly underestimated from the CESM
560 model. Using WRF/Chem or its variant, Zhang et al. (2016b, 2019) found that the column CO
561 performance could be greatly improved by adjusting the BCON using the satellite observation. A
562 similar approach could be applied in future WRF-CMAQ simulations as well. Second, as pointed
563 by Heald et al. (2003), the regional emissions, especially biomass burning, could be a significant
564 source for elevated CO concentrations and thus underestimation of these emissions could
565 contribute to the CO underprediction. A more robust set of fire emissions from FINN generated
566 by NCAR based on satellite retrievals has been applied to the similar time period recently but

Formatted: Subscript

567 using the WRF-Chem model (Zhang and Wang, 2019) and were found to improve the column
568 CO performance. Last, Emmons et al. (2009) showed positive biases (i.e., 19%) of MOPITT
569 retrievals over the land when compared to in-situ measurements and the biases may have been
570 increasing over time due to the MOPITT bias drift (e.g., 0.5% yr⁻¹ for version 7 retrieval). The
571 predicted TOR can capture the observed high values over the eastern U.S. and oceans and the
572 low values in elevated terrain especially in summer; and it shows the best performance among all
573 gas species. Both satellite observations and simulations can capture the elevated column NO₂
574 over the industrial and metropolitan areas in the domain where large nitrogen oxide (NO_x)
575 emission sources are located especially in winter. The model shows moderate underprediction
576 with an NMB of -27.8% in summer which can be attributed to both uncertainties in the emissions
577 and satellite retrievals. For example, the lightning emissions of NO_x are missing from this study,
578 which have been found by previous studies (Allen et al., 2012) to contribute up to 2.0×10^{15}
579 molecules cm⁻² over the southern U.S., the Gulf of Mexico, and northern Atlantic Ocean during
580 ~~certain episodes~~ the summer. Boersma et al. (2004) also found that different column NO₂
581 retrieval approaches may lead to large errors (> 25%) over polluted areas. Column HCHO over
582 the CONUS especially the southeastern U.S. is well predicted in summer in terms of both
583 magnitude and spatial distribution and correlates well with the biogenic emission source regions.
584 The underprediction of column HCHO in winter may ~~thus~~ indicate potential underestimation of
585 ~~biogenic emissions from the BEIS~~ anthropogenic emissions. Other reasons including potential
586 low yield of HCHO from isoprene and terpene in the CB05 mechanism and uncertainties in
587 satellite retrievals (Stavrakou et al., 2009; Lorente et al., 2017)

588 **3.2.4 Simulated O₃ and PM_{2.5} exceedances of NAAQS levels**

589 National Ambient Air Quality Standards (NAAQS) are set for criteria pollutants,
590 including O₃ and PM_{2.5}, to provide protection against adverse health and welfare effects
591 (www.epa.gov/criteria-air-pollutants/naaqs-table). In this section, the average number of days
592 per year where the 24-hr PM_{2.5} NAAQS level (35 µg m⁻³) and the max 8-h O₃ NAAQS level (70
593 ppb) are exceeded from the WRF-CMAQ predictions is compared with the number of
594 exceedances in the monitoring data (i.e., O₃ from AQS and CASTNET and PM_{2.5} from
595 IMPROVE and CSN). This comparison is intended to better characterize the ability of the model
596 to simulate the high-concentration days that could be especially relevant in regulatory
597 assessments. In Figure 148, the five-year average of the annual number of exceedance days is
598 shown for WRF-CMAQ and the monitoring data at monitor locations. ~~The sizes of circles and
599 shades of color represent the magnitude of exceedances (i.e., larger circles and darker shades
600 indicate a greater number of exceedance days).~~ As shown, the observations indicate a large
601 number of annual exceedance days for max 8-h O₃ over major cities, especially in CA, TX, the
602 Midwest, and northeastern U.S. The spatial distribution of the observed number of exceedance
603 days from the AQS and CASTNET networks aligns well with the nonattainment map reported by
604 the Green Book of U.S. EPA (<https://www.epa.gov/green-book>). The WRF-CMAQ model also
605 ~~generally~~ captures the distribution of the number of exceedance days very well, especially in CA
606 ~~and northeastern U.S.~~ The domain-average values of NMB, NME, and R are -3.4%, 14.0%, and
607 0.98, respectively, also indicating a good performance. For PM_{2.5}, the largest number of
608 exceedance days based on the IMPROVE and CSN observations mainly occurs in the
609 northwestern U.S., Midwest, and major cities in the northeastern U.S. The number of exceedance
610 days is generally much lower for PM_{2.5} than O₃. The spatial distribution of the number of
611 exceedance days for observed PM_{2.5} aligns well with nonattainment areas reported by the Green

612 Book from U.S. EPA in CA. However, the number of simulated PM_{2.5} exceedance days
613 underpredicts the observation-based values in the western U.S. mainly due to large
614 underpredictions of PM_{2.5} concentrations in the same areas as shown in Figure 106a. The
615 simulation better predicts the distribution of the number of exceedance days in the eastern U.S.
616 where terrain is relatively flat and wildfire less prevalent. The domain-average values of NMB,
617 NME, and R are -29.0%, 80.8%, and 0.21, respectively.

618 **4. Impacts of chemistry-meteorology feedbacks**

619 In this section, the impacts of chemistry-meteorology feedbacks including aerosol direct
620 and indirect effects on regional meteorology and air quality over the U.S. are further examined
621 by comparing results from two-way WRF-CMAQ and offline coupled WRF and CMAQ. Model
622 performance from the two sets of simulations is first compared to demonstrate the potential
623 performance improvements of the two-way model, and the impacts on regional meteorology and
624 air quality are further investigated via the spatial difference plots for selected variables and
625 species.

626 **4.1 Meteorology**

627 Figures 24 and 84 compare observations and simulations from the two-way WRF-CMAQ
628 and WRF-only models for precipitation and SWCF/LWCF, respectively. Tables 1 and 2 also
629 summarize the model performance statistics for all major meteorological variables for the two
630 simulations. The statistics of some cloud variables from the WRF-only simulation are not
631 available due to missing model outputs. Overall, good performance is evident for both
632 simulations for surface meteorological variables with slightly better performance for most of
633 variables (except for RH2 in both seasons and T2 in summer) for the two-way WRF-CMAQ

634 simulation than the WRF-only simulation. The MBs for the two-way WRF-CMAQ vs. WRF-
635 only simulation are 10.1 °C vs 10.2 °C for T2, 2.2% vs 2.14-8% for RH2, 0.5744 m s⁻¹ vs 0.5846
636 m s⁻¹ for WS10, 16.732.8 degree vs 16.933.4 degree for WD10, and 0.0514-0.71 mm day⁻¹ vs
637 0.042-0.728 mm day⁻¹ for precipitation in winter and -1.1 °C vs -0.9 °C for T2, 3.7% vs 3.2% for
638 RH2, 0.38 m s⁻¹ vs 0.42 m s⁻¹ for WS10, 49.1 degree vs 49.8 degree for WD10, and 0.13-0.75
639 mm day⁻¹ vs 0.19-0.9 mm day⁻¹ for precipitation in summer. The spatial distributions for SWCF
640 and LWCF are slightly-better captured in both seasons especially over the eastern U.S., Atlantic
641 Ocean, and Gulf of Mexico in winter and over the Midwest, Atlantic Ocean, and Pacific
642 Northwest in summerregions. Compared to WRF-only, two-way WRF-CMAQ shows noticeably
643 better performance in terms of both MB and RMSE for radiation and cloud forcing, with MBs of
644 11.337.0 vs. 19.524.2 W m⁻² for SWDOWN, 728.5 vs 14.17.6 W m⁻² for GSW, -0.940.6 vs. -
645 6.34 W m⁻² for GLW, 4.02.8 vs. 4.72.0 W m⁻² for OLR, -3.047.6 vs. -7.440.7 W m⁻² for SWCF,
646 and -3.35.9 vs. -4.15.3 W m⁻² for LWCF in winter and with MBs of 43.6 vs. 59.4 W m⁻² for
647 SWDOWN, 33.6 vs 47.2 W m⁻² for GSW, -13.4 vs. -16.8 W m⁻² for GLW, 2.3 vs. 3.0 W m⁻² for
648 OLR, -22.8 vs. -31.1 W m⁻² for SWCF, and -8.6 vs. -9.0 W m⁻² for LWCF in summer. These
649 results are consistent with those reported by Yahaya et al. (2015a,b) that showed similar
650 improvements in meteorological and radiative variables when comparing predictions from WRF-
651 Chem with those from WRF only. Since identical inputs and physics options are used in both
652 simulations, the differences in performance for meteorological variables is due to the
653 consideration of feedback processes among chemistry, aerosol, cloud, and radiation in the two-
654 way coupled WRF-CMAQ simulation.

655 Figure 159 shows the 5-year average difference plots of selected major meteorological
656 variables including SWDOWN, T2, RH2, WS10, PBL height, and precipitation between two-

657 way WRF-CMAQ and WRF-only [in 2008-2012](#). As shown, the incoming shortwave radiation is
658 reduced by up to 24.8 W m^{-2} (13.6%) with a domain-average of 13.0 W m^{-2} (6%) due to the
659 combined aerosol direct and indirect radiative effects over the domain. The reduction is
660 predominant over the eastern U.S. where both aerosol loading and cloud cover are high and over
661 the oceans where cloud cover is high. The magnitude of shortwave radiation reduction in this
662 work is consistent with other studies. For example, Wang et al. (2015a) found that the combined
663 aerosol direct and indirect effects using the WRF/Chem model, which includes the sub-scale
664 cloud forcing not treated in the current WRF-CMAQ model, may decrease the incoming
665 shortwave radiation by 16.0 W m^{-2} in the summer over the U.S. Hogrefe et al. (2015) reported
666 the reduction of shortwave radiation may reach up to 20 W m^{-2} over the eastern U.S. by only
667 considering the aerosol direct effect using an older version of WRF-CMAQ v5.0.1. Xing et al.
668 (2015b) showed that the aerosol direct forcing may cause the surface shortwave radiation to
669 decrease by up to 10 W m^{-2} over the eastern U.S. over a decadal time period using WRF-CMAQ
670 v5.0. The reduction of shortwave radiation further reduces the surface temperature by up to
671 $0.25 \text{ }^\circ\text{C}$ over the eastern U.S., which is much larger than the reduction of $0.1 \text{ }^\circ\text{C}$ reported by
672 Hogrefe et al. (2015), mainly due to the inclusion of aerosol indirect effects. However there are
673 smaller reductions of T2 over the Pacific Ocean and even increases (by up to $0.1 \text{ }^\circ\text{C}$) over large
674 areas of Atlantic Ocean and Gulf of Mexico where much larger reductions of shortwave radiation
675 occur. As pointed by Wang et al. (2015a), due to the much larger heat capacity of ocean, the
676 response of sea surface temperature is less sensitive to the change of shortwave radiation for
677 ocean compared to the land. The large increase of incoming longwave radiation and latent heat
678 (figures not shown) caused by the aerosol indirect effects and other complex feedback processes
679 over the ocean compensates for the reduction of shortwave radiation, especially over the Atlantic

680 Ocean and Gulf of Mexico, and thus leads to less reduction or even increases of T2. RH2 is
681 found to mostly increase by 3.4% over the land caused by the decrease of temperature while
682 decrease by 2.6% over the ocean caused by either the increase of temperature or large decrease
683 of water vapor. Over the land, the decreases in ~~solar shortwave~~ radiation and ~~temperature T2~~
684 along with the latent heat (figure not shown) lead to a more stable PBL and thus suppress the
685 wind (by reducing the wind speed as shown). Over the ocean, the changes lead to a more
686 unstable PBL and thus enhance the wind over the ocean. The wind speed and PBL height are
687 reduced by up to 0.05 m s⁻¹ and 25 m, respectively, over the U.S. The aerosol feedbacks on
688 precipitation are also mixed with relatively large decreases by up to 0.4 mm day⁻¹ over the U.S.
689 and increases by up to 0.4 mm day⁻¹ over oceans. The suppression of precipitation over the land
690 is mainly due to the formation of more small sized CCNs caused by aerosol indirect effects and
691 align well with areas with high aerosol loadings while the enhancement of precipitation,
692 especially along coastlines and over oceans, might be associated with the larger CCN formation
693 via more activated sea-salt particles as indicated by Zhang et al. (2010) and Wang et al. (2015a).

694 **4.2 Air Quality**

695 Figures ~~9-11~~ ~~5 and 6~~ compare observations and simulations from two-way WRF-CMAQ
696 and offline CMAQ for O₃, PM_{2.5}, and PM_{2.5} constituents. Tables ~~3 and 4~~ ~~2~~ summarizes the
697 statistics for all major chemical variables for the two simulations. As shown in Figure ~~9~~ ~~5~~, two-
698 way WRF-CMAQ shows better performance for both the monthly variation of O₃ (throughout
699 the whole year) over AQS sites and the diurnal pattern of O₃ (especially during winter) over
700 CASTNET sites due to better performance of T2 and radiation compared to offline WRF and
701 CMAQ. As shown in Figure ~~10~~ ~~6~~, two-way WRF-CMAQ shows ~~better similar~~ spatial distribution
702 of PM_{2.5} ~~in winter and similar one in summer~~ and better performance for PM_{2.5} for most of

703 months over CSN sites and for cold seasons across IMPROVE sites compared to offline CMAQ.
704 ~~It also~~Figure 11 shows systematically better performance for SO_4^{2-} , NO_3^- , NH_4^+ , and TC with
705 more data within 1:2 ~~and~~ closer to 1:1 ratio lines of scatter plots in both seasons. Overall, as
706 shown in Tables 3 and 42, both simulations show generally good performance for all major
707 chemical species except for PM_{10} . For example., the domain-average NMBs are 102.6% (AQS)
708 and -3.04-5% (CASTNET) vs. 147.27% (AQS) and 0.27-7% (CASTNET) for O_3 in summer, and
709 -7.20% (CSN) and 8.6-13.7% (IMPROVE) vs. -1.83-4% (CSN) and 23.7-5.7% (IMPROVE) for
710 $\text{PM}_{2.5}$ in winter and -13.2% (CSN) and -26.9% (IMPROVE) vs. -14.0% (CSN) and -22.8%
711 (IMPROVE) for $\text{PM}_{2.5}$ in summer for two-way WRF-CMAQ and offline-coupled CMAQ,
712 respectively. The two-way WRF-CMAQ shows better domain-wide statistics in terms of both
713 correlation and biases for many variables including O_3 , SO_4^{2-} , NO_3^- , ~~NH_4^+~~ , and EC as well as
714 TOR and column NO_2 in both seasons, apparently due to the treatment of chemistry-meteorology
715 feedbacks. Offline CMAQ performs better for total $\text{PM}_{2.5}$ especially in the western U.S. due to
716 higher dust emissions from higher wind speed and higher SOA due to stronger radiation and
717 higher temperature. However more robust comparisons are needed in the future with improved
718 dust emissions and the use of FINN wildfire emissions.

719 Figure 160 shows the 5-year average difference plots of selected chemical variables
720 including CO, O_3 , NO_x , volatile organic compounds (VOCs), SO_4^{2-} , SOA, $\text{PM}_{2.5}$, and PM_{10}
721 between two-way WRF-CMAQ and offline-coupled CMAQ. As shown, the CO mixing ratios
722 decrease by up to 79.2 ppb (27.8%) especially over the western U.S. with a domain-average
723 reduction of 3.0 ppb (3.1%) due to reduced formation of CO from the oxidation of VOCs caused
724 by reduced solar radiation as indicated by Zhang et al. (2017). Such reductions seem to dominate
725 over the increases caused by reduced PBL height, especially in the western U.S. where PBL

726 height reductions are minimum. The O₃ mixing ratios decrease by up to 5.2 ppb (16.2%) with
727 domain-average of 1.7 ppb (4.2%) mainly due to the reduced solar radiation and T2. The change
728 of O₃ is consistent with other studies such as Makar et al. (2015) and Wang et al. (2015a) that
729 also reported lower O₃ mixing ratios caused by aerosol direct and indirect effects. On the other
730 hand, both NO_x and VOC mixing ratios increase over the eastern U.S. while they decrease over
731 the western U.S. The increase should be caused by the combination of the large reduction of PBL
732 mixing and reduced solar radiation which reduces NO₂ photolysis and VOC oxidation to SOA.
733 For aerosol species, SO₄²⁻ concentrations increase by up to 0.38 μg m⁻³ (26.6%) especially over
734 the eastern U.S. In fact, the ~~reduction-decrease~~ of O₃ mixing ratios ~~due to aerosol effects~~
735 ~~caused~~ ~~by feedbacks~~ is expect~~ing~~ed to reduce SO₄²⁻ production via the gas-phase oxidation pathway due
736 to the influence of O₃ on OH, but increase SO₄²⁻ production via the aqueous-phase chemistry
737 pathway due to more clouds in the two-way WRF-CMAQ simulation. Thus, the net increase of
738 SO₄²⁻ is more dominate by the aqueous-phase chemistry instead of the gas-phase oxidation. This
739 net increase of SO₄²⁻, in turn, leads to an increase of NH₄⁺ and decrease of NO₃⁻ (figures not
740 shown) through aerosol thermodynamic equilibrium. SOA concentrations decrease by up to 0.34
741 μg m⁻³ (41.6%) especially over the eastern U.S. due to the large reduction of oxidants. PM_{2.5}
742 concentrations also decrease by up to 5.2 μg m⁻³ (49.1%) with a domain-average of 0.34 μg m⁻³
743 (8.6%), and PM₁₀ concentrations decrease by up to 19.3 μg m⁻³ (64.8%) with a domain-average
744 of 1.1 μg m⁻³ (11.1%). The reductions are more apparent over the western U.S. than the eastern
745 U.S. partially due to the compensation of the increase of SO₄²⁻ and NH₄⁺ and decrease of other
746 secondary aerosols over the eastern U.S., as well as the relatively large reduction of dust
747 concentrations over the western U.S. caused by reduced wind speed.

748 5. Summary and conclusion

749 In this study, two sets of long-term simulations for 2008-2012 using the two-way coupled
750 WRF-CMAQ and offline coupled WRF and CMAQ, respectively, are conducted, evaluated, and
751 compared to investigate the performance improvements due to chemistry-meteorology feedbacks
752 and impacts of those feedbacks on the regional air quality in the U.S. First, the two-way coupled
753 WRF-CMAQ simulation with both aerosol direct and indirect radiative forcing is
754 comprehensively evaluated in both winter and summer seasons and the annual trend is examined
755 between observations and simulations for selected major variables. The results show that WRF-
756 CMAQ performs well for major surface meteorological variables such as temperature at 2 m,
757 relative humidity at 2 m, wind speed at 10 m, and precipitation with domain-average MBs of \pm
758 1.1-1.10 °C, 2.2-3.7%, 0.38-0.5744 m s⁻¹, and 0.134-0.2328 mm day⁻¹ (except for 0.71-0.75
759 mm day⁻¹ against NCDC), respectively, in winter and summer. The overall small warm bias
760 compared to other studies is most likely associated with the soil moisture nudging technique used
761 in the PX land surface scheme. The relatively large positive biases for precipitation are found to
762 be more apparent when observed precipitation is low (dominated more by the non-convective
763 precipitation) and are thus believed to be more associated with uncertainties in the Morrison
764 microphysics scheme. The long-term simulation also shows generally good performance for
765 major radiation and cloud radiative variables. Relatively large model biases still exist for cloud
766 variables such as CDNC, COT, and CWP, indicating that the processes associated with aerosol
767 indirect effects are still not well understood and an accurate simulation of those effects is still
768 challenging using state-of-the-science models. WRF-CMAQ can also capture the observed year-
769 to-year variations well for almost all the major meteorological and chemical variables.

770 Two-way WRF-CMAQ also shows generally good or acceptable performance for max 8-
771 h O₃, PM_{2.5} and PM_{2.5} constituents, with NMBs generally within $\pm 15\%$ for O₃ and $\pm 30\%$ for

772 PM_{2.5} species. For example, the domain-average NMBs are 102.6 % and ~~-3.045~~ % for max 8-h
773 O₃ against AQS and CASTNET in summer and ~~-13.2 to -7.20~~ % and ~~-26.9 to 8.643-7~~ % for
774 PM_{2.5} against CSN and IMPROVE, respectively in both seasons. O₃ mixing ratios are
775 overpredicted for most months, especially in the winter, in part due to the larger overprediction
776 of T2 during the cold season. The overall model biases are small for PM_{2.5} due to the
777 compensation of relatively large underpredictions of SO₄²⁻ and OC, especially in the warm
778 season, and overprediction of NO₃⁻ in the cold season. In addition to biases inherited from the
779 meteorology, the model performance for chemistry also suffers from uncertainties associated
780 with emissions, the use of a coarse spatial resolution, and representation of aerosol formation
781 pathways in the model. For example, the relatively large biases for EC might be associated with
782 poorly allocated anthropogenic/wildfire emissions and those for OC might be due to
783 underestimation of SOA formation in version 5.0.2 of CMAQ. WRF-CMAQ also predicts the
784 column abundances of chemical species well and the relatively large model biases for CO are
785 found to be associated with an underestimation of BCONs. The model better reproduces the
786 observed number of exceedance days for O₃ than PM_{2.5} mainly due to better performance for O₃
787 than PM_{2.5} concentrations.

788 The performance comparison between two-way WRF-CMAQ and WRF-only simulations
789 shows that two-way WRF-CMAQ model performs better for major surface meteorological,
790 radiation, and cloud radiative variables due to the consideration of chemistry-meteorology
791 feedbacks associated with aerosol direct and indirect forcing. The feedbacks are found to reduce
792 the 5-year average SWDOWN by up to 24.8 W m⁻², T2 by up to 0.25 °C, PBL height by up to 25
793 m, wind speed by up to 0.05 m s⁻¹, and precipitation by up to 0.4 mm day⁻¹ over the CONUS,
794 which in turn affect the air quality significantly. As a result of feedbacks, two-way WRF-CMAQ

795 outperforms offline CMAQ for O_3 , SO_4^{2-} , NO_3^- , NH_4^+ , and EC as well as TOR and column NO_2
796 in terms of both spatiotemporal variations and domain-average statistics due to better
797 meteorology performance for variables such as T2, WS10, radiation, and precipitation. Despite
798 these improvements, the offline CMAQ performs better for total $PM_{2.5}$ in terms of domain-
799 average statistics, which could be partially caused by the compensation of larger under- and
800 over-predictions of $PM_{2.5}$ constituents. More robust comparison for $PM_{2.5}$ should be performed
801 with improved dust and wildfire emissions in future work. Chemistry-meteorology feedbacks are
802 found to play important roles in affecting U.S. air quality by reducing domain-wide 5-year
803 average surface CO by 3.0 ppb (3.1%) and up to 79.2 ppb (27.8%), O_3 by 1.7 ppb (4.1%) and up
804 to 5.2 ppb (16.2%), $PM_{2.5}$ by $0.34 \mu g m^{-3}$ (8.6%) and up to $5.2 \mu g m^{-3}$ (49.1%), and PM_{10} by 1.1
805 $\mu g m^{-3}$ (11.1%) and up to $19.3 \mu g m^{-3}$ (64.8%) mainly due to reduction of radiation, temperature,
806 and wind speed.

807 In summary, the two-way coupled WRF-CMAQ modeling in this study shows generally
808 satisfactory and consistent performance for the long-term prediction of regional meteorology and
809 air quality when compared to other studies in the literature. Possible causes for the
810 meteorological and chemical biases that were identified through this work can provide valuable
811 information for future model development to improve the two-way coupled WRF-CMAQ model
812 and those biases should also be considered when making future climate/air quality projections.
813 Non-negligible model improvements for many major meteorological and chemical variables
814 compared to the traditional application of offline coupled WRF and CMAQ suggest the
815 importance of chemistry-meteorology feedbacks, especially aerosol direct and indirect effects.
816 The feedbacks should be considered along with other factors in developing future model
817 applications to inform policy making.

818 **Code Availability**

819 The modeling system used in this study is based on the 2-way coupled WRF-CMAQ model
820 derived from WRF v3.4 and CMAQ v5.0.2. Relevant code for CMAQ v5.0.2, its coupling to
821 WRF and aerosol direct feedbacks are publicly available from: doi:10.5281/zenodo.1079898.
822 WRF v3.4 code can be downloaded from
823 http://www2.mmm.ucar.edu/wrf/users/download/get_source.html. The version of the coupled
824 WRF-CMAQ model with the additional indirect aerosol forcing approach of Yu et al. (2014) can
825 be downloaded from the following website: <https://person.zju.edu.cn/shaocaiyu#674502>.

826 **Author contribution**

827 YZ and MB defined the scope of the manuscript. YZ and KW designed ~~the study and~~ all the
828 simulations. SY and DW developed the two-way coupled WRF-CMAQ code. KW conducted all
829 the simulations and performed the analyses. KW ~~prepared-drafted~~ the manuscript. YZ, SY, DW,
830 JP, RM, JK, and MB reviewed and edited the manuscript.
831 ~~with contributions from all co-authors.~~

832 **Competing interests**

833 The authors declare that they have no conflict of interest.

834 **Acknowledgements**

835 This work was developed at North Carolina State University and Northeastern University under
836 Assistance Agreement No. RD835871 awarded by the U.S. Environmental Protection Agency to
837 Yale University. The views expressed in this manuscript are those of the authors alone and do
838 not necessarily reflect the views and policies of the U.S. Environmental Protection Agency. EPA

839 does not endorse any products or commercial services mentioned in this publication. High
840 performance computing was support from Yellowstone (ark:/85065/d7wd3xhc) provided by
841 NCAR's CISL, sponsored by the NSF and the Stampede XSEDE high-performance computing
842 support under the NSF ACI-1053575. The work of S. Yu is supported by the Department of
843 Science and Technology of China (No. 2016YFC0202702, 2018YFC0213506 and
844 2018YFC0213503), National Research Program for Key Issues in Air Pollution Control in China
845 (No. DQGG0107) and National Natural Science Foundation of China (No. 21577126 and
846 41561144004). The authors gratefully acknowledge the availability of CERES, GPCP, MODIS,
847 MOPITT, NCDC, OMI, PRISM, SCHIAMACHY, and TMPA data. The authors thank Dr. Ralf
848 Bennartz from Vanderbilt University for providing the CDNC data. The authors also would like
849 to thank Drs. Jerry Herwehe and Shannon Koplitz from the U.S. EPA for their constructive and
850 very helpful comments.

851 **References**

- 852 Abdul-Razzak, H. and Ghan, S. J.: A parameterization of aerosol activation 2. Multiple aerosol
853 types, *J. Geophys. Res.*, 105 (D3), 6837-6844, 2000.
- 854 Alapaty, K., Herwehe, J. A., Otte, T. L., Nolte, C. G., Bullock, O. R., Mallard, M. S., Kain, J. S.,
855 and Dudhia, J.: Introducing subgrid-scale cloud feedbacks to radiation for regional
856 meteorological and climate modeling, *Geophys. Res. Lett.*, 39, L24809,
857 <https://doi.org/10.1029/2012GL054031>, 2012.
- 858 Allen, D. J., Pickering, K. E., Pinder, R. W., Henderson, B. H., Appel, K. W., and Prados, A.:
859 Impact of lightning-NO on eastern United States photochemistry during the summer of 2006 as
860 determined using the CMAQ model, *Atmos. Chem. Phys.*, 12, 1737-
861 1758, <https://doi.org/10.5194/acp-12-1737-2012>, 2012.
- 862 Appel, K. W., Gilliland, A. B., Sarwar, G., and Gilliam, R. C.: Evaluation of the Community
863 Multiscale Air Quality (CMAQ) model version 4.5: Sensitivities impacting model performance:
864 Part I, Ozone, *Atmos. Environ.*, 41, 9603-9615, 2007.
- 865 Appel, K. W., Pouliot, G. A., Simon, H., Sarwar, G., Pye, H. O. T., Napelenok, S. L., Akhtar, F.,
866 and Roselle, S. J.: Evaluation of dust and trace metal estimates from the Community Multiscale

867 Air Quality (CMAQ) model version 5.0, *Geosci. Model Dev.*, 6, 883–899,
868 <https://doi.org/10.5194/gmd-6-883-2013>, 2013.

869 Appel, K. W., Napelenok, S. L., Foley, K. M., Pye, H. O. T., Hogrefe, C., Luecken, D. J., Bash,
870 J. O., Roselle, S. J., Pleim, J. E., Foroutan, H., Hutzell, W. T., Pouliot, G. A., Sarwar, G., Fahey,
871 K. M., Gantt, B., Gilliam, R. C., Heath, N. K., Kang, D., Mathur, R., Schwede, D. B., Spero, T.
872 L., Wong, D. C., and Young, J. O.: Description and evaluation of the Community Multiscale Air
873 Quality (CMAQ) modeling system version 5.1, *Geosci. Model Dev.*, 10, 1703–1732,
874 <https://doi.org/10.5194/gmd-10-1703-2017>, 2017.

875 Baklanov, A., Schlünzen, K. H., Suppan, P., Baldasano, J., Brunner, D., Aksoyoglu, S.,
876 Carmichael, G., Douros, J., Flemming, J., Forkel, R., Galmarini, S., Gauss, M., Grell, G., Hirtl,
877 M., Joffre, S., Jorba, O., Kaas, E., Kaasik, M., Kallos, G., Kong, X., Korsholm, U., Kurganski,
878 A., Kushta, J., Lohmann, U., Mahura, A., Manders-Groot, A., Maurizi, A., Moussiopoulos, N.,
879 Rao, S. T., Savage, N., Seigneur, C., Sokhi, R. S., Solazzo, E., Solomos, S., Sørensen, B.,
880 Tsegas, G., Vignati, E., Vogel, B., and Zhang, Y.: Online coupled regional meteorology-
881 chemistry models in Europe: Current status and prospects, *Atmos. Chem. Phys.*, 14, 317–398,
882 [doi:10.5194/acp-14-317-2014](https://doi.org/10.5194/acp-14-317-2014), 2014.

883 Bennartz, R.: Global assessment of marine boundary layer cloud droplet number concentration
884 from satellite, *J. Geophys. Res.*, 112, D02201, <http://dx.doi.org/10.1029/2006JD007547>, 2007.

885 Boersma, K. F., Eskes, H. J., and Brinksma, E. J.: Error analysis for tropospheric NO₂ retrieval
886 from space, *J. Geophys. Res.*, 109, D04311, [doi:10.1029/2003JD003962](https://doi.org/10.1029/2003JD003962), 2004.

887 Brunner, D., Savage, N., Jorba, O., Eder, B., Giordano, L., Badia, A., Balzarini, A., Baro, R.,
888 Bianconi, R., Chemel, C., Curci, G., Forkel, R., Jimenez-Guerrero, P., Hirtl, M., Hodzic, A.,
889 Hozak, L., Im, U., Knote, C., Makar, P., Manders-Groot, A., van Meijgaard, E., Neal, L., Perez,
890 J. L., Pirovano, G., San Jose, R., Schroder, W., Sokhi, R. S., Syrakov, D., Torian, A., Tuccella,
891 P., Werhahn, J., Wolke, R., Yahya, K., Zabkar, R., Zhang, Y., Hogrefe, C., and Galmarini, S.:
892 Comparative analysis of meteorological performance of coupled chemistry-meteorology models
893 in the context of AQMEII phase 2, *Atmos. Environ.*, 115, 470–498,
894 [doi:10.1016/j.atmosenv.2014.12.032](https://doi.org/10.1016/j.atmosenv.2014.12.032), 2015.

895 Byun, D. W. and Schere K. L.: Review equations, computational algorithms, and other
896 components of the Models-3 Community Multi-Scale Air Quality (CMAQ) modeling system,
897 *Applied Mechanics Reviews*, 59(2), 51–77, [doi:10.1115/1.2128636](https://doi.org/10.1115/1.2128636), 2006.

898 Choi, M.W., Lee, J. H., Woo, J. W., Kim, C. H., and Lee, S. H.: Comparison of PM_{2.5} chemical
899 components over East Asia simulated by the WRF-Chem and WRF/CMAQ models: On the
900 models' prediction inconsistency, *Atmosphere*, 10, 618, 2019.

901 Cohen, A. E., Cavallo, S. M., Coniglio, M. C., and Brooks, H. E.: A review of planetary
902 boundary layer parameterization schemes and their sensitivity in simulating southeastern U.S.
903 cold season severe weather environments, *Weather and Forecasting*,
904 <https://doi.org/10.1175/WAF-D-14-00105.1>, 2015.

905 Dong, X., Fu, J. S., Huang, K., Tong, D., and Zhuang, G.: Model development of dust emission
906 and heterogeneous chemistry within the Community Multiscale Air Quality modeling system

907 and its application over East Asia, *Atmos. Chem. Phys.*, 16, 8157–8180,
908 <https://doi.org/10.5194/acp-16-8157-2016>, 2016.

909 Eder, B. and Yu, S.: A performance evaluation of the 2004 release of Models-3 CMAQ, *Atmos.*
910 *Environ.*, 40(26):4811-4824, 2006.

911 Emery, C., Liu, Z., Russell, A. G., Odman, M. T., Yarwood, G., and Kumar, N.:
912 Recommendations on statistics and benchmarks to assess photochemical model performance, *J.*
913 *Air Waste Manage. Assoc.*, 67:5, 582-598, doi:10.1080/10962247.2016.1265027, 2017.

914 Emmons, L. K., Edwards, D. P., Deeter, M. N., Gille, J. C., Campos, T., Nédélec, P., Novelli, P.,
915 and Sachse, G.: Measurements of Pollution In The Troposphere (MOPITT) validation through
916 2006, *Atmos. Chem. Phys.*, 9, 1795–1803, <https://doi.org/10.5194/acp-9-1795-2009>, 2009.

917 ~~Foroutan, H., Young, J., Napelenok, S., Ran, L., Appel, K. W., Gilliam, R. C., and Pleim, J. E.:~~
918 ~~Development and evaluation of a physics-based windblown dust emission scheme implemented~~
919 ~~in the CMAQ modeling system, *J. Adv. Model. Earth Syst.*, 9, 585–608,~~
920 ~~doi:10.1002/2016MS000823, 2017.~~

921 Gan, C.-M., Pleim, J., Mathur, R., Hogrefe, C., Long, C. N., Xing, J., Wong, D., Gilliam, R., and
922 Wei, C.: Assessment of long-term WRF–CMAQ simulations for understanding direct aerosol
923 effects on radiation "brightening" in the United States, *Atmos. Chem. Phys.*, 15, 12193–12209,
924 <https://doi.org/10.5194/acp-15-12193-2015>, 2015a.

925 Gan, C.-M., Binkowski, F., Pleim, J., Xing, J., Wong, D., Mathur, R., and Gilliam, R.:
926 Assessment of the aerosol optics component of the coupled WRF–CMAQ model using CARES
927 field campaign data and a single column model, *Atmos. Environ.*, 115, 670-682, 2015b.

928 Gantt, B., He, J., Zhang, X., Zhang, Y., and Nenes, A.: Incorporation of advanced aerosol
929 activation treatments into CESM/CAM5: model evaluation and impacts on aerosol indirect
930 effects, *Atmos. Chem. Phys.*, 14, 7485–7497, <https://doi.org/10.5194/acp-14-7485-2014>, 2014.

931 Gantt, B., Sarwar, G., Xing, J., Simon, H., Schwede, D., Hutzell, W. T., Mathur, R., and Saiz-
932 Lopez, A.: The impact of iodide-mediated ozone deposition and halogen chemistry on surface
933 ozone concentrations across the continental United States, *Environ. Sci. Technol.*, 51 (3), 1458-
934 1466, 2017.

935 Ghan, S. J., Laulainen, N. S., Easter, R. C., Wagener, R., Nemesure, S., Chapman, E. G., Zhang,
936 Y., and Leung, L. R.: Evaluation of aerosol direct radiative forcing in MIRAGE, *J. Geophys.*
937 *Res.*, 106, 5295–5316, 2001.

938 Glotfelty, T., He, J., and Zhang, Y.: Impact of future climate policy scenarios on air quality and
939 aerosol-cloud interactions using an advanced version of CESM/CAM5: Part I. model evaluation
940 for the current decadal simulations, *Atmos. Environ.*, 152, 222-239, 2017.

941 Grell, G. A., Peckham, S. E., Schmitz, R., McKenn, S. A., Frost, G., Skamarock, W. C., and
942 Eder, B.: Fully Coupled "Online" chemistry within the WRF Model, *Atmos. Environ.*, 39, 6957–
943 6975, 2005.

944 Grell, G. A. and Baklanov, A.: Integrated modelling for forecasting weather and air quality: A
945 call for fully coupled approaches, *Atmos. Environ.*, 45, 38, 6845–6851, 2011.

946 He, J. and Zhang, Y.: Improvement and further development in CESM/CAM5: Gasphase
947 chemistry and inorganic aerosol treatments, *Atmos. Chem. Phys.*, 14, 9171-9200,
948 <http://dx.doi.org/10.5194/acp-14-9171-2014>, 2014.

949 Heald, C. L., Jacob, D. J., Fiore, A. M., Emmons, L. K., Gille, J. C., Deeter, M. N., Warner, J.,
950 Edwards, D. P., Crawford, J. H., Hamlin, A. J., Sachse, G. W., Browell, E. V., Avery, M. A.,
951 Vay, S. A., Westberg, D. J., Blake, D. R., Singh, H. B., Sandholm, S. T., Talbot, R. W., and
952 Fuelberg, H. E.: Asian outflow and trans-Pacific transport of carbon monoxide and ozone
953 pollution: An integrated satellite, aircraft, and model perspective, *J. Geophys. Res.*, 108(D24),
954 4804, doi:10.1029/2003JD003507, 2003.

955 Herwehe, J. A., Otte, T. L., Mathur, R., and Rao, S. T.: Diagnostic analysis of ozone
956 concentrations simulated by two regional-scale air quality models, *Atmos. Environ.*, 45, 5957–
957 5969, 2011.

958 Hogrefe, C., Pouliot, G., Wong, D., Torian, A., Roselle, S., Pleim, J., and Mathur, R.: Annual
959 application and evaluation of the online coupled WRF–CMAQ system over North America
960 under AQMEII phase 2, *Atmos. Environ.*, 115, 683-694, 2015.

961 Hong, C., Zhang, Q., Zhang, Y., Tang, Y., Tong, D., and He, K.: Multi-year downscaling
962 application of two-way coupled WRF v3.4 and CMAQ v5.0.2 over east Asia for regional climate
963 and air quality modeling: model evaluation and aerosol direct effects, *Geosci. Model Dev.*, 10,
964 2447–2470, <https://doi.org/10.5194/gmd-10-2447-2017>, 2017.

965 Hong, C.-P., Zhang, Q., Zhang, Y., Davis, S. J., Zhang, X., Tong, D., Guan, D., Liu, Z., and He,
966 K.-B.: Weakened aerosol radiative effects may mitigate the climate penalty on Chinese air
967 quality, *Nature Climate Change*, in press, 2020.

968 Iacono, M. J., Delamere, J. S., Mlawer, E. J., Shephard, M. W., Clough, S. A., and Collins, W.
969 D.: Radiative forcing by long-lived greenhouse gases: Calculations with the AER radiative
970 transfer models, *J. Geophys. Res. Atmos.*, 113, D13103, <https://doi.org/10.1029/2008JD009944>,
971 2008.

972 IPCC: Global warming of 1.5°C, An IPCC Special Report on the impacts of global warming of
973 1.5°C above pre-industrial levels and related global greenhouse gas emission pathways, in the
974 context of strengthening the global response to the threat of climate change, sustainable
975 development, and efforts to eradicate poverty edited by Masson-Delmotte, V., Zhai, P., Pörtner,
976 H. O., Roberts, D., Skea, J., Shukla, P. R., Pirani, A., Moufouma-Okia, W., Péan, C., Pidcock,
977 R., Connors, S., Matthews, J. B. R., Chen, Y., Zhou, X., Gomis, M. I., Lonnoy, E., Maycock, T.,
978 Tignor, M., and Waterfield, T., 2018.

979 Jacobson, M. Z., Lu, R., Turco, R. P., and Toon, O. B.: Development and application of a new
980 air pollution modeling system. Part I: Gas-phase simulations, *Atmos. Environ.*, 30B, 1939–1963,
981 1996.

982 Jacobson, M. Z.: GATOR-GCMM: A global- through urban-scale air pollution and weather
983 forecast model 1. Model design and treatment of subgrid soil, vegetation, roads, rooftops, water,
984 sea, ice, and snow, *J. Geophys. Res.*, 106, 5385–5401, 2001.

985 Jung, J., Souri, A. H., Wong, D. C., Lee, S., Jeon, W., Kim, J., and Choi, Y.: The impact of the
986 direct effect of aerosols on meteorology and air quality using aerosol optical depth assimilation
987 during the KORUS - AQ campaign, *J. Geophys. Res. Atmos.*, 124, 8303–8319,
988 <https://doi.org/10.1029/2019JD030641>, 2019.

989 Kain, J. S.: The Kain-Fritsch convective parameterization: An update, *J. Appl. Meteorol.*, 43,
990 170–181, [https://doi.org/10.1175/1520-0450\(2004\)043<0170:TKCPAU>2.0.CO;2](https://doi.org/10.1175/1520-0450(2004)043<0170:TKCPAU>2.0.CO;2), 2004.

991 Karydis, V. A., Tsimpidi, A. P., and Pandis, S. N.: Evaluation of a three-dimensional chemical
992 transport model (PMCAMx) in the eastern United States for all four seasons, *J. Geophys. Res.*,
993 112, D14211, doi:10.1029/2006JD007890, 2007.

994 Kaufman, Y. J., Smirnov, A., Holben, B., and Dubovik, O.: Baseline maritime aerosol
995 methodology to derive the optical thickness and scattering properties, *Geophys. Res. Lett.*, 28,
996 3251, doi:10.1029/2001GL013312, 2001.

997 Kelly, J., Koplitz, S., Baker, K., Holder, A., Pye, H., Murphy, B., Bash, J., Henderson, B.,
998 Possiel, N., Simon, H., Eyth, A., Jang, C., Phillips, S., and Timin, B.: Assessing PM_{2.5} model
999 performance for the conterminous U.S. with comparison to model performance statistics from
1000 2007-2015, *Atmos. Environ.*, 214, <https://doi.org/10.1016/j.atmosenv.2019.116872>, 2019.

1001 Kukkonen, J., Olsson, T., Schultz, D. M., Baklanov, A., Klein, T., Miranda, A. I., Monteiro, A.,
1002 Hirtl, M., Tarvainen, V., Boy, M., Peuch, V.-H., Poupkou, A., Kioutsioukis, I., Finardi, S.,
1003 Sofiev, M., Sokhi, R., Lehtinen, K. E. J., Karatzas, K., San José, R., Astitha, M., Kallos, G.,
1004 Schaap, M., Reimer, E., Jakobs, H., and Eben, K.: A review of operational, regional-scale,
1005 chemical weather forecasting models in Europe, *Atmos. Chem. Phys.*, 12, 1–87,
1006 doi:10.5194/acp-12-1-2012, 2012.

1007 Li, P., Wang, L., Guo, P., Yu, S., Mehmood, K., Wang, S., Liu, W., Seinfeld, J. H., Zhang, Y.,
1008 Wong, D., Alapaty, K., Pleim, J., and Mathur, R.: High reduction of ozone and particulate matter
1009 during the 2016 G-20 summit in Hangzhou by forced emission controls of industry and traffic,
1010 *Environ. Chem. Lett.*, 15:709–715, doi:10.1007/s10311-017-0642-2, 2017.

1011 Lin, M., Holloway, T., Carmichael, G. R., and Fiore, A. M.: Quantifying pollution inflow and
1012 outflow over East Asia in spring with regional and global models, *Atmos. Chem. Phys.*, 10,
1013 4221–4239, <https://doi.org/10.5194/acp-10-4221-2010>, 2010.

1014 Liu, X.-H., Zhang, Y., Xing, J., Zhang, Q., Wang, K., Streets, D. G., Jang, C. J., Wang, W.-X.,
1015 and Hao, J. M.: Understanding of regional air pollution over China using CMAQ:- Part II.
1016 Process analysis and ozone sensitivity to precursor emissions, *Atmos. Environ.*, 44(20), 3719-
1017 3727, 2010.

1018 Lorente, A., Folkert Boersma, K., Yu, H., Dörner, S., Hilboll, A., Richter, A., Liu, M., Lamsal,
1019 L. N., Barkley, M., De Smedt, I., Van Roozendaal, M., Wang, Y., Wagner, T., Beirle, S., Lin, J.-
1020 T., Krotkov, N., Stammes, P., Wang, P., Eskes, H. J., and Krol, M.: Structural uncertainty in air

1021 mass factor calculation for NO₂ and HCHO satellite retrievals, *Atmos. Meas. Tech.*, 10, 759–
1022 782, <https://doi.org/10.5194/amt-10-759-2017>, 2017.

1023 Ma, P.-L., Rasch, P. J., Fast, J. D., Easter, R. C., Gustafson Jr., W. I., Liu, X., Ghan, S. J., and
1024 Singh, B.: Assessing the CAM5 physics suite in the WRF-Chem model: implementation,
1025 resolution sensitivity, and a first evaluation for a regional case study, *Geosci. Model Dev.*, 7,
1026 755–778, <https://doi.org/10.5194/gmd-7-755-2014>, 2014.

1027 Makar, P., A., Gong, W., Hogrefe, C., Zhang, Y., Curci, G., Žabkar, R., Milbrandt, J., Im, U.,
1028 Balzarini, A., Baró, R., Bianconi, R., Cheung, P., Forkel, R., Gravel, S., Hirtl, M., Honzak, L.,
1029 Hou, A., Jiménez-Guerrero, P., Langer, M., Moran, M. B., Pabla, B., Pérez, J. L., Pirovano, G.,
1030 San José, R., Tuccella, P., Werhahn, J., Zhang, J., and Galmarini, S.: Feedbacks between air
1031 pollution and weather, Part 2: Effects on chemistry, *Atmos. Environ.*, 115, 499–526, 2015.

1032 Mathur, R., Xiu, A., Coats, C., Alapaty, K., Shankar, U., and Hanna, A.: Development of an air
1033 quality modeling system with integrated meteorology, chemistry, and emissions, *Proc.*
1034 *Measurement of Toxic and Related Air Pollutants*, AWMA, Cary, NC, September, 1998.

1035 Mathur, R., Xing, J., Gilliam, R., Sarwar, G., Hogrefe, C., Pleim, J., Pouliot, G., Roselle, S.,
1036 Spero, T. L., Wong, D. C., and Young, J.: Extending the Community Multiscale Air Quality
1037 (CMAQ) modeling system to hemispheric scales: overview of process considerations and initial
1038 applications, *Atmos. Chem. Phys.*, 17, 12449–12474, 2017.

1039 Matsui, H., Koike, M., Kondo, Y., Takegawa, N., Kita, K., Miyazaki, Y., Hu, M., Chang, S.-Y.,
1040 Blake, D. R., Fast, J. D., Zaveri, R. A., Streets, D. G., Zhang, Q. and Zhu, T.: Spatial and
1041 temporal variations of aerosols around Beijing in summer 2006: Model evaluation and source
1042 apportionment, *J. Geophys. Res.*, 114, D00G13, doi:10.1029/2008JD010906, 2009.

1043 Mebust, M. R., Eder, B. K., Binkowski, F. S., and Roselle, S. J.: Models-3 Community
1044 Multiscale Air Quality (CMAQ) model aerosol component: 2. Model evaluation, *J. Geophys.*
1045 *Res.*, 108(D6), 4184, doi:10.1029/2001JD001410, 2003.

1046 Mehmood, K., Wu, Y., Wang, L., Yu, S., Li, P., Chen, X., Li, Z., Zhang, Y., Li, M., Liu, W.,
1047 Wang, Y., Liu, Z., Zhu, Y., Rosenfeld, D., and Seinfeld, J. H.: Relative effects of open biomass
1048 burning and open crop straw burning on haze formation over central and eastern China:
1049 modeling study driven by constrained emissions, *Atmos. Chem. Phys.*, 20, 2419–2443,
1050 <https://doi.org/10.5194/acp-20-2419-2020>, 2020.

1051 Morrison, H., Thompson, G., and Tatarskii, V.: Impact of cloud microphysics on the
1052 development of trailing stratiform precipitation in a simulated squall line: Comparison of one-
1053 and two-moment schemes, *Mon. Weather Rev.*, 137, 991–1007,
1054 <https://doi.org/10.1175/2008MWR2556.1>, 2009.

1055 Penrod, A., Zhang, Y., Wang, K., Wu, S.-Y., and Leung, R. L.: Impacts of future climate and
1056 emission changes on US air quality, *Atmos. Environ.*, 89, 533–547,
1057 doi:10.1016/j.atmosenv.2014.01.001, 2014.

1058 Pleim, J. E.: A combined local and nonlocal closure model for the atmospheric boundary layer.
1059 Part I: Model description and testing, *J. Appl. Meteorol. Clim.*,
1060 <https://doi.org/10.1175/JAM2539.1>, 2007.

1061 Pleim, J., Young, J., Wong, D., Gilliam, R., Otte, T., and Mathur, R.: Two-way coupled
1062 meteorology and air quality modeling, in *Air Pollution Modeling and its Application*, edited by
1063 C. Borrego and A. I. Miranda, XIX, NATO Science for Peace and Security Series, Series C:
1064 Environmental Security, Springer, Dordrecht, 2008.

1065 Pleim, J. E. and Gilliam, R.: An indirect data assimilation scheme for deep soil temperature in
1066 the Pleim–Xiu land surface model, *J. Appl. Meteorol. Clim.*, 48, 1362–1376, 2009.

1067 Pye, H. O. T., Murphy, B. N., Xu, L., Ng, N. L., Carlton, A. G., Guo, H., Weber, R., Vasilakos,
1068 P., Appel, K. W., Budisulistiorini, S. H., Surratt, J. D., Nenes, A., Hu, W., Jimenez, J. L.,
1069 Isaacman-VanWertz, G., Misztal, P. K., and Goldstein, A. H.: On the implications of aerosol
1070 liquid water and phase separation for organic aerosol mass, *Atmos. Chem. Phys.*, 17, 343–369,
1071 doi:10.5194/acp-17-343-2017, 2017.

1072 Pye, H. O. T., Nenes, A., Alexander, B., Ault, A. P., Barth, M. C., Clegg, S. L., Collett Jr., J. L.,
1073 Fahey, K. M., Hennigan, C. J., Herrmann, H., Kanakidou, M., Kelly, J. T., Ku, I.-T., McNeill, V.
1074 F., Riemer, N., Schaefer, T., Shi, G., Tilgner, A., Walker, J. T., Wang, T., Weber, R., Xing, J.,
1075 Zaveri, R. A., and Zuend, A.: The acidity of atmospheric particles and clouds, *Atmos. Chem.*
1076 *Phys.*, 20, 4809–4888, <https://doi.org/10.5194/acp-20-4809-2020>, 2020.

1077 Remer, L. A., Kaufman, Y. J., Tanré, D., Mattoo, S., Chu, D. A., Martins, J. V., Li, R. R.,
1078 Ichoku, C., Levy, R. C., and Kleidman, R. G.: The MODIS aerosol algorithm, products, and
1079 validation, *J. Atmos. Sci.*, 62, 947–973, 2005.

1080 Roy, B., Pouliot, G. A., Gilliland, A., Pierce, T., Howard, S., Bhave, P. V., and Benjey, W.:
1081 Refining fire emissions for air quality modeling with remotely sensed fire counts: A wildfire case
1082 study, *Atmos. Environ.*, 41(3), 655–665, doi:10.1016/j.atmosenv.2006.08.037, 2007.

1083 San Joaquin Valley Air Pollution Control District: 2018 Plan for the 1997, 2006, and 2012 PM_{2.5}
1084 Standards, November 15, 2018, <https://www.valleyair.org/pmplans>, 2018.

1085 Sarwar, G., Luecken, D., Yarwood, G., Whitten, G. Z., and Carter, W. P. L.: Impact of an
1086 updated carbon bond mechanism on predictions from the CMAQ modeling system: Preliminary
1087 assessment, *J. Appl. Meteor. Clim.*, 47, 3e14, 2008.

1088 Sarwar, G., Gantt, B., Schwede, D., Foley, K., Mathur, R., and Saiz-Lopez, A.: Impact of
1089 enhanced ozone deposition and halogen chemistry on tropospheric ozone over the Northern
1090 Hemisphere, *Environ. Sci. Technol.*, 49 (15), 9203–9211, 2015.

1091 Scheffe, R. D., Strum, M., Phillips, S. B., Thurman, J., Eyth, A., Fudge, S., Morris, M., Palma,
1092 T., and Cook, R.: Hybrid modeling approach to estimate exposures of hazardous air pollutants
1093 (HAPs) for the National Air Toxics Assessment (NATA), *Environ. Sci. Technol.*, 2016, 50(22),
1094 12356–12364, doi:10.1021/acs.est.6b04752, 2016.

1095 Schwede, D., Pouliot, G. A., and Pierce, T.: Changes to the biogenic emissions inventory system
1096 version 3 (BEIS3), in: Proceedings of the 4th CMAS Models-3 Users' Conference, Chapel Hill,
1097 NC, 26–28 September, 2005.

1098 Sekiguchi, A., Shimadera, H., and Kondo, A.: Impact of aerosol direct effect on wintertime
1099 PM_{2.5} simulated by an online coupled meteorology-air quality model over East Asia, *Aerosol.*
1100 *Air Qual. Res.*, 18, 1068–1079, 2018.

1101 Solazzo, E., Hogrefe, C., Colette, A., Garcia-Vivanco, M., and Galmarini, S.: Advanced error
1102 diagnostics of the CMAQ and Chimere modelling systems within the AQMEII3 model
1103 evaluation framework, *Atmos. Chem. Phys.*, 17, 10435–10465, 2017.

1104 U.S. EPA: Policy assessment for the review of the National Ambient Air Quality Standards for
1105 particulate matter, EPA-452/R-20-002, January 2020,
1106 [https://www.epa.gov/sites/production/files/2020-](https://www.epa.gov/sites/production/files/2020-01/documents/final_policy_assessment_for_the_review_of_the_pm_naaqs_01-2020.pdf)
1107 [01/documents/final_policy_assessment_for_the_review_of_the_pm_naaqs_01-2020.pdf](https://www.epa.gov/sites/production/files/2020-01/documents/final_policy_assessment_for_the_review_of_the_pm_naaqs_01-2020.pdf), 2020.

1108 Vasilakos, P., Russell, A., Weber, R., and Nenes, A.: Understanding nitrate formation in a world
1109 with less sulfate. *Atmos. Chem. Phys.* 18, 12765–12775, 2018.

1110 Wang, K. and Zhang, Y.: Application, evaluation, and process analysis of U.S. EPA's 2002
1111 multiple-pollutant air quality modeling platform, *Atmospheric and Climate Sciences*, 2, 254–289,
1112 2012.

1113 Wang, K. and Zhang, Y.: 3-D agricultural air quality modeling: Impacts of NH₃/H₂S gas-phase
1114 reactions and bi-directional exchange of NH₃, *Atmos. Environ.*, 98, 554–570, doi:
1115 10.1016/j.atmosenv.2014.09.010, 2014.

1116 Wang, K., Zhang, Y., Jang, C., Phillips, S., and Wang, B.: Modeling intercontinental air
1117 pollution transport over the trans-Pacific region in 2001 using the Community Multiscale Air
1118 Quality modeling system, *J. Geophys. Res.*, 114, D04307, doi:10.1029/2008JD010807, 2009.

1119 Wang, K., Zhang, Y., Nenes, A., and Fountoukis, C.: Implementation of dust emission and
1120 chemistry into the Community Multiscale Air Quality modeling system and initial application to
1121 an Asian dust storm episode, *Atmos. Chem. Phys.*, 12, 10209–10237,
1122 <https://doi.org/10.5194/acp-12-10209-2012>, 2012.

1123 Wang, J., Wang, S., Jiang, J., Ding, A., Zheng, M., Zhao, B., Wong, C.-D., Zhou, W., Zheng, G.,
1124 Wang, L., Pleim, J., and Hao, J.: Impact of aerosol–meteorology interactions on fine particle
1125 pollution during China's severe haze episode in January 2013, *Environ. Res. Lett.*, 9,
1126 doi:10.1088/1748-9326/9/9/094002, 2014.

1127 Wang, K., Zhang, Y., Yahya, K., Wu, S.-Y., and Grell, G.: Implementation and initial
1128 application of new chemistry-aerosol options in WRF/Chem for simulating secondary organic
1129 aerosols and aerosol indirect effects for regional air quality, *Atmos. Environ.*, 115, 716–732,
1130 doi:10.1016/j.atmosenv.2014.12.007, 2015a.

1131 [Wang, K., Yahya, K., Zhang, Y., Hogrefe, C., Pouliot, G., Knote, C., Hodzic, A., Jose, R. S.,](#)
1132 [Perez, J. L., Jiménez-Guerrero, P., Baro, R., Makar, P., and Bennartz, R.: A multi-model](#)

1133 [assessment for the 2006 and 2010 simulations under the Air Quality Model Evaluation](#)
1134 [International Initiative \(AQMEII\) Phase 2 over North America: Part II. Evaluation of column](#)
1135 [variable predictions using satellite data, Atmos. Environ., 115, 1–17,](#)
1136 [10.1016/j.atmosenv.2014.07.044, 2015b.](#)

1137 [Wang, K., Zhang, Y., and Yahya, K.: Decadal application of WRF/Chem over the continental](#)
1138 [U.S.: Simulation design, sensitivity simulations, and climatological model evaluation, Atmos.](#)
1139 [Environ., 118331, doi: 10.1016/j.atmosenv.2021.118331, 2021.](#)

1140 West, J. J., Ansari, A. S., and Pandis, S. N.: Marginal PM_{2.5}: Nonlinear aerosol mass response to
1141 sulfate reductions in the Eastern United States, *J. Air Waste Manage. Assoc.*, 49, 1415–1424,
1142 <https://doi.org/10.1080/10473289.1999.10463973>, 1999.

1143 Wiedinmyer, C., Quayle, B., Geron, C., Belote, A., McKenzie, D., Zhang, X., O’Neill, S., and
1144 Wynne, K. K.: Estimating emissions from fires in North America for air quality modeling,
1145 *Atmos. Environ.*, 40(19): 3419–32, doi:10.1016/j.atmosenv.2006.02.010, 2006.

1146 Wielicki, B. A., Barkstrom, B. R., Harrison, E. F., Lee III, R. B., Smith, G. L., and Cooper, J. E.:
1147 Clouds and the Earth’s Radiant Energy System (CERES): An earth observing system
1148 experiment, *B. Am. Meteorol. Soc.*, 77, 853–868, 1996.

1149 Wilczak, J. M., Djalalova, I., McKeen, S., Bianco, L., Bao, J.-W., Grell, G., Peckham, S.,
1150 Mathur, R., McQueen, J., and Lee, P.: Analysis of regional meteorology and surface ozone during
1151 the TexAQS II field program and an evaluation of the NMM-CMAQ and WRF-Chem air quality
1152 models, *J. Geophys. Res.*, 114, D00F14, 2009.

1153 Wong, D. C., Pleim, J., Mathur, R., Binkowski, F., Otte, T., Gilliam, R., Pouliot, G., Xiu, A.,
1154 Young, J. O., and Kang, D.: WRFCMAQ two-way coupled system with aerosol feedback:
1155 Software development and preliminary results, *Geosci. Model Dev.*, 5, 299–312,
1156 <https://doi.org/10.5194/gmd-5-299-2012>, 2012.

1157 Xing, J., Mathur, R., Pleim, J., Hogrefe, C., Gan, C.-M., Wong, D. C., Wei, C., and Wang, J.: Air
1158 pollution and climate response to aerosol direct radiative effects: A modeling study of decadal
1159 trends across the northern hemisphere, *J. Geophys. Res. Atmos.*, 120, 12,221–12,236,
1160 doi:10.1002/2015JD023933, 2015a.

1161 Xing, J., Mathur, R., Pleim, J., Hogrefe, C., Gan, C.-M., Wong, D. C., and Wei, C.: Can a
1162 coupled meteorology–chemistry model reproduce the historical trend in aerosol direct radiative
1163 effects over the Northern Hemisphere?, *Atmos. Chem. Phys.*, 15, 9997–10018,
1164 <https://doi.org/10.5194/acp-15-9997-2015>, 2015b.

1165 Xing, J., Wang, J., Mathur, R., Pleim, J., Wang, S., Hogrefe, C., Gan, C.-M., Wong, D., and Hao,
1166 J.: Unexpected benefits of reducing aerosol cooling effects, *Environ. Sci. Technol.*, 50, 7527–
1167 7534, <https://doi.org/10.1021/acs.est.6b00767>, 2016.

1168 Xing, J., Wang, J., Mathur, R., Wang, S., Sarwar, G., Pleim, J., Hogrefe, C., Zhang, Y., Jiang, J.,
1169 Wong, D. C., and Hao, J.: Impacts of aerosol direct effects on tropospheric ozone through
1170 changes in atmospheric dynamics and photolysis rates, *Atmos. Chem. Phys.*, 17, 9869–9883,
1171 <https://doi.org/10.5194/acp-17-9869-2017>, 2017.

- 1172 Xiu, A. and Pleim, J. E.: Development of a land surface model. Part I: Application in a
 1173 mesoscale meteorological model, *J. Appl. Meteorol.*, 40, 192–209, <https://doi.org/10.1175/1520->
 1174 0450(2001)040<0192:doalsm>2.0.co;2, 2001.
- 1175 Yahya, K., Wang, K., Gudoshava, M., Glotfelty, T., and Zhang, Y.: Application of WRF/Chem
 1176 over North America under the AQMEII Phase 2. Part I. Comprehensive evaluation of 2006
 1177 simulation, *Atmos. Environ.*, 115, 733-755, doi:10.1016/j.atmosenv.2014.08.063, 2015a.
- 1178 Yahya, K., Wang, K., Zhang, Y., and Kleindienst, T. E.: Application of WRF/Chem over North
 1179 America under the AQMEII Phase 2 – Part 2: Evaluation of 2010 application and responses of
 1180 air quality and meteorology–chemistry interactions to changes in emissions and meteorology
 1181 from 2006 to 2010, *Geosci. Model Dev.*, 8, 2095–2117, <https://doi.org/10.5194/gmd-8-2095->
 1182 2015, 2015b.
- 1183 Yahya, K., Wang, K., Campbell, P., Glotfelty, T., He, J., and Zhang, Y.: Decadal evaluation of
 1184 regional climate, air quality, and their interactions over the continental US and their interactions
 1185 using WRF/Chem version 3.6.1, *Geosci. Model Dev.*, 9, 671–695, <https://doi.org/10.5194/gmd->
 1186 9-671-2016, 2016.
- 1187 Yarwood, G., Rao, S., Yocke, M., and Whitten, G. Z.: Final Report–Updates to the Carbon Bond
 1188 Chemical Mechanism: CB05, Rep.RT-04-00675, Yocke and Co., Novato, Calif., 246 pp., 2005.
- 1189 Yoo, J.-W., Jeon, W., Park, S.-Y., Park, C., Jung, J., Lee, S.-H., and Lee, H. W.: Investigating
 1190 the regional difference of aerosol feedback effects over South Korea using the WRF-CMAQ
 1191 two-way coupled modeling system, *Atmos. Environ.*, 218, 116968, 2019.
- 1192 Yu, S., Eder, B., Dennis, R., Chu, S., and Schwartz, S.: New unbiased symmetric metrics for
 1193 evaluation of air quality models, *Atmos. Sci. Lett.*, 7, 26-34, 2006.
- 1194 Yu, S. C., Mathur, R., Schere, K., Kang, D., Pleim, J., and Otte, T. L.: A detailed evaluation of
 1195 the Eta-CMAQ forecast model performance for O₃, its related precursors, and meteorological
 1196 parameters during the 2004 ICARTT Study, *J. Geophys. Res.*, 112, D12S14,
 1197 doi:10.1029/2006JD007715, 2007.
- 1198 Yu, S. C., Mathur, R., Pleim, J., Wong, D., Carlton, A. G., Roselle, S., and Rao, S. T.:
 1199 Simulation of the indirect radiative forcing of climate due to aerosols by the two-way coupled
 1200 WRF-CMAQ over the eastern United States, in *Air Pollution Modeling and its Applications*,
 1201 edited by D. G. Steyn and S. T. Castelli, XXI, Springer Netherlands, Netherlands, C(96), 579–
 1202 583, 2011.
- 1203 Yu, S., Mathur, R., Pleim, J., Wong, D., Gilliam, R., Alapaty, K., Zhao, C., and Liu, X.: Aerosol
 1204 indirect effect on the grid-scale clouds in the two-way coupled WRF–CMAQ: Model
 1205 description, development, evaluation and regional analysis, *Atmos. Chem. Phys.*, 14, 11247–
 1206 11285, <https://doi.org/10.5194/acp-14-11247-2014>, 2014.
- 1207 Yu, S., Li, P., Wang, L., Wu, Y., Wang, S., Liu, W., Zhu, T., Zhang, Y., Hu, M., Alapaty, K.,
 1208 Wong, D., Pleim, J., Mathur, R., Rosenfeld, D., and Seinfeld, J.: Mitigation of severe urban haze
 1209 pollution by a precision air pollution control approach, *Scientific Reports*, 8:8151,
 1210 doi:10.1038/s41598-018-26344-1, 2018.

1211 Yu, X.-Y., Lee, T., Ayres, B., Kreidenweis, S. M., Malm, W., and Collett, J. L.: Loss of fine
1212 particle ammonium from denuded nylon filters, *Atmos. Environ.*, 40, 4797-4807, 2006.

1213 [Zender, C. S., H. Bian, and D. Newman: Mineral Dust Entrainment and Deposition \(DEAD\)](#)
1214 [model: Description and 1990s dust climatology, *J. Geophys. Res.*, 108, 4416,](#)
1215 [doi:10.1029/2002JD002775, 2003.](#)

1216 Zhang, Y.: Online coupled meteorology and chemistry models: History, current status, and
1217 outlook, *Atmos. Chem. Phys.*, 8, 2895-2932, doi:10.5194/acp-8-2895-2008, 2008.

1218 [Zhang, Y. and Wang, Y.: Climate-driven ground-level ozone extreme in the fall over the](#)
1219 [Southeast United States, *P. Natl. Acad. Sci. USA*, 113, 10025–10030,](#)
1220 <https://doi.org/10.1073/pnas.1602563113>, 2016.

1221 Zhang, Y. and Wang, K.: Project 3 - Air quality and climate modeling: Multi-model application,
1222 evaluation, intercomparison, and ensemble over the U.S., poster presentation at the Air Climate
1223 Energy (ACE) Centers Meeting, Pittsburgh, PA, June 18-19, 2019.

1224 Zhang, K. M., Knipping, E. M., Wexler, A. S., Bhave, P. V., and Tonnesen, G. S.: Size
1225 distribution of sea-salt emissions as a function of relative humidity, *Atmos. Environ.*, 39, 3373-
1226 3379, 2005.

1227 Zhang, Y., Liu, P., Pun, B., and Seigneur, C.: A comprehensive performance evaluation of MM5-
1228 CMAQ for the summer 1999 Southern Oxidants Study episode, Part-I. Evaluation protocols,
1229 databases and meteorological predictions, *Atmos. Environ.*, 40, 4825-4838,
1230 doi:10.1016/j.atmosenv.2005.12.043, 2006.

1231 Zhang, Y., Vijayaraghavan, K., Wen, X.-Y., Snell, H. E., and Jacobson, M. Z.: Probing into
1232 regional ozone and particulate matter pollution in the United States: 1. A 1-year CMAQ
1233 simulation and evaluation using surface and satellite data, *J. Geophys. Res.*, 114, D22304,
1234 doi:10.1029/2009JD011898, 2009a.

1235 Zhang, Y., Wen, X.-Y., Wang, K., Vijayaraghavan, K., and Jacobson, M. Z.: Probing into
1236 regional ozone and particulate matter pollution in the United States: 2. An examination of
1237 formation mechanisms through a process analysis technique and sensitivity study, *J. Geophys.*
1238 *Res.*, 114, D22305, doi:10.1029/2009JD011900, 2009b.

1239 Zhang, Y., Wen, X.-Y., and Jang C. J.: Simulating chemistry-aerosol-cloud-radiation-climate
1240 feedbacks over the continental US using the online-coupled Weather Research Forecasting
1241 Model with chemistry (WRF/Chem), *Atmos. Environ.*, 44(29), 3568-3582, doi:
1242 10.1016/j.atmosenv.2010.05.056, 2010.

1243 Zhang, Y., Sartelet, K., Zhu, S., Wang, W., Wu, S.-Y., Zhang, X., Wang, K., Tran, P., Seigneur,
1244 C., and Wang, Z.-F.: Application of WRF/Chem-MADRID and WRF/Polyphemus in Europe –
1245 Part 2: Evaluation of chemical concentrations and sensitivity simulations, *Atmos. Chem. Phys.*,
1246 13, 6845–6875, <https://doi.org/10.5194/acp-13-6845-2013>, 2013.

1247 Zhang, Y., Chen, Y., Fan, J., and Leung, L. R.: Application of an online-coupled regional
1248 climate model, WRF-CAM5, over East Asia for examination of ice nucleation schemes: Part II.

- 1249 Sensitivity to ice nucleation parameterizations and dust emissions, *Climate*, 3(3), 753-774,
1250 doi:10.3390/cli3030753, 2015a.
- 1251 Zhang, Y., Zhang, X., Wang, K., He, J., Leung, L. R., Fan, J.-W., and Nenes, A.: Incorporating
1252 an advanced aerosol activation parameterization into WRF-CAM5: Model evaluation and
1253 parameterization intercomparison, *J. Geophys. Res.*, 120 (14), doi:10.1002/2014JD023051,
1254 2015b.
- 1255 Zhang, Y., Zhang, X., Wang, L., Zhang, Q., Duan, F., and He, K.: Application of WRF/Chem
1256 over East Asia: Part I. Model evaluation and intercomparison with MM5/CMAQ, *Atmos.*
1257 *Environ.*, 124, 285–300, 2016a.
- 1258 Zhang, Y., Hong, C.-P., Yahya, K., Li, Q., Zhang, Q., and He, K.-B.: Comprehensive evaluation
1259 of multi-year real-time air quality forecasting using an online-coupled meteorology-chemistry
1260 model over southeastern United States, *Atmos. Environ.*, 138, 162-182,
1261 doi:10.1016/j.atmosenv.2016.05.006, 2016b.
- 1262 Zhang, Y., Wang, K., and He J.: Multi-year application of WRF-CAM5 over East Asia-Part II:
1263 Interannual variability, trend analysis, and aerosol indirect effects, *Atmos. Environ.*, 165, 222-
1264 239, 2017.
- 1265 Zhang, Y., Jena, C., Wang, K., Paton-Walsh, C., Guérette, E.-A., Utembe, S., Silver, J. D., and
1266 Keywood, M.: Multiscale applications of two online-coupled meteorology-chemistry models
1267 during recent field campaigns in Australia, Part I: Model description and WRF/Chem-ROMS
1268 evaluation using surface and satellite data and sensitivity to spatial grid resolutions, *Atmosphere*,
1269 10(4), 189, doi:10.3390/atmos10040189, 2019.
- 1270 Zheng, B., Zhang, Q., Zhang, Y., He, K. B., Wang, K., Zheng, G. J., Duan, F. K., Ma, Y. L., and
1271 Kimoto, T.: Heterogeneous chemistry: a mechanism missing in current models to explain
1272 secondary inorganic aerosol formation during the January 2013 haze episode in North China,
1273 *Atmos. Chem. Phys.*, 15, 2031–2049, <https://doi.org/10.5194/acp-15-2031-2015>, 2015.

Table 1. The 5-year average performance statistics for meteorological variables between two-way WRF-CMAQ and WRF-only simulations in winter, 2008-2012.

Variables	Datasets	Mean Obs	Two-way WRF-CMAQ					WRF-only				
			Mean Sim	R	MB	NMB (%)	RMSE	Mean Sim	R	MB	NMB (%)	RMSE
T2 (°C)	NCDC	7.5	8.6	0.97	1.1	14.9	1.6	8.6	0.97	1.2	15.8	1.6
RH2 (%)		72.9	75.1	0.79	2.2	3.0	6.3	75.0	0.79	2.1	2.8	6.3
WS10 (m s ⁻¹)		3.93	4.50	0.4	0.57	14.6	1.17	4.50	0.4	0.58	14.6	1.17
WD10 (deg)		166.4	183.1	0.0	16.7	10.0	44.2	183.3	0.0	16.9	10.2	44.4
Precipitation (mm day ⁻¹)	NCDC	1.54	2.25	0.46	0.71	46.3	1.94	2.26	0.47	0.72	47.0	1.94
	NADP	2.48	2.68	0.77	0.2	8.0	1.14	2.69	0.77	0.21	8.6	1.14
	GPCP	1.81	2.04	0.80	0.23	12.8	1.03	2.04	0.80	0.23	12.8	1.02
	PRISM	1.91	2.08	0.89	0.17	9.0	0.79	2.09	0.89	0.18	9.4	0.79
	TMPA	2.02	2.07	0.81	0.05	2.4	1.01	2.06	0.81	0.04	2.0	1.02
SWDOWN (W m ⁻²)	CERES	108.5	119.8	0.99	11.3	10.4	13.7	128.0	0.98	19.5	17.9	22.2
GSW (W m ⁻²)		87.1	94.6	0.99	7.5	8.6	10.1	101.3	0.98	14.1	16.2	17.1
GLW (W m ⁻²)		278.9	278.0	0.99	-0.9	-0.3	5.9	272.7	0.99	-6.3	-2.2	8.6
OLR (W m ⁻²)		222.3	226.2	0.99	4.0	1.8	5.1	227.0	0.99	4.7	2.1	5.8
SWCF (W m ⁻²)		-26.6	-23.6	0.91	-3.0	-11.1	6.3	-19.2	0.85	-7.4	-27.8	10.6
LWCF (W m ⁻²)		22.0	18.7	0.76	-3.3	-15.1	6.0	18.0	0.72	-4.1	-18.4	6.7
AOD	MODIS	0.11	0.04	0.44	-0.06	-59.8	0.08	N/A	N/A	N/A	N/A	N/A
CF		0.66	0.59	0.87	-0.07	-10.4	0.1	N/A	N/A	N/A	N/A	N/A
CDNC (cm ⁻³)		172.3	30.4	0.21	-141.9	-82.4	157.5	N/A	N/A	N/A	N/A	N/A
CWP (g m ⁻²)		177.4	97.0	0.63	-80.4	-45.3	93.2	N/A	N/A	N/A	N/A	N/A
COT		16.9	3.3	0.74	-13.6	-80.8	14.2	N/A	N/A	N/A	N/A	N/A

* outputs of AOD, CF, CDNC, CWP, and COT are not available from WRF-only simulations

Table 2. The 5-year average performance statistics for meteorological variables between two-way WRF-CMAQ and WRF-only simulations in summer, 2008-2012.

Variables	Datasets	Mean Obs	Two-way WRF-CMAQ					WRF-only				
			Mean Sim	R	MB	NMB (%)	RMSE	Mean Sim	R	MB	NMB (%)	RMSE
T2 (°C)		22.3	22.2	0.95	-1.1	-4.6	1.7	22.4	0.95	-0.9	-3.7	1.6
RH2 (%)	NCDC	67.0	70.7	0.91	3.7	5.5	6.6	70.1	0.91	3.2	4.7	6.3
WS10 (m s ⁻¹)		3.19	3.57	0.36	0.38	11.8	0.99	3.61	0.35	0.42	13.1	1.01
WD10 (deg)		146.4	195.4	0.0	49.1	33.5	67.3	196.1	0.0	49.8	34.0	67.9
		2.11	2.86	0.5	0.75	35.6	1.93	3.01	0.5	0.9	42.6	2.01
Precipitation (mm day ⁻¹)	NADP	2.82	2.99	0.83	0.17	5.9	0.87	3.14	0.83	0.32	11.2	0.93
	GPCP	2.55	2.78	0.80	0.23	9.0	1.19	2.86	0.80	0.30	11.9	1.21
	PRISM	2.35	2.55	0.89	0.20	8.4	0.69	2.65	0.89	0.30	12.9	0.73
	TMPA	2.70	2.83	0.80	0.13	4.8	1.27	2.89	0.81	0.19	6.8	1.27
SWDOWN (W m ⁻²)		254.7	298.3	0.84	43.6	17.1	46.6	314.1	0.73	59.4	23.3	62.8
GSW (W m ⁻²)		222.5	256.1	0.75	33.6	15.1	37.6	269.7	0.57	47.2	21.2	51.7
GLW (W m ⁻²)	CERES	372.2	358.8	0.98	-13.4	-3.6	15.3	355.4	0.98	-16.8	-4.5	18.7
OLR (W m ⁻²)		257.2	259.6	0.96	2.3	0.9	4.8	260.2	0.96	3.0	1.2	5.2
SWCF (W m ⁻²)		-55.1	-32.3	0.69	-22.8	-41.3	27.6	-24.0	0.50	-31.1	-56.4	36.2
LWCF (W m ⁻²)		26.1	17.5	0.85	-8.6	-33.0	9.8	17.1	0.87	-9.0	-34.6	10.0
AOD		0.20	0.07	0.67	-0.13	-67.8	0.14	N/A	N/A	N/A	N/A	N/A
CF		0.53	0.41	0.81	-0.12	-23.0	0.16	N/A	N/A	N/A	N/A	N/A
CDNC (cm ⁻³)	MODIS	138.9	28.9	0.11	-110.0	-79.2	124.1	N/A	N/A	N/A	N/A	N/A
CWP (g m ⁻²)		162.2	54.6	0.65	-107.6	-66.3	113.8	N/A	N/A	N/A	N/A	N/A
COT		14.2	2.3	0.73	-11.9	-83.6	12.2	N/A	N/A	N/A	N/A	N/A

* outputs of AOD, CF, CDNC, CWP, and COT are not available from WRF-only simulations

Table 3. The 5-year average performance statistics for chemical variables between two-way WRF-CMAQ and offline CMAQ simulations in winter, 2008-2012.

Variables	Datasets	Mean Obs	Two-way WRF-CMAQ					Offline CMAQ				
			Mean Sim	R	MB	NMB (%)	NME (%)	Mean Sim	R	MB	NMB (%)	NME (%)
Max 8-hr O ₃ (ppb)	AQS	32.4	39.6	0.61	7.2	22.5	23.0	42.3	0.65	9.9	30.7	30.9
	CASTNET	34.9	36.6	0.76	1.7	4.9	9.4	39.7	0.75	4.7	13.5	14.3
PM _{2.5} (µg m ⁻³)	CSN	11.4	10.6	0.21	-0.8	-7.2	29.3	11.7	0.2	0.21	1.8	31.0
	IMPROVE	3.59	3.90	0.83	0.31	8.6	30.3	4.44	0.86	0.85	23.7	32.1
PM ₁₀ (µg m ⁻³)	AQS	19.9	12.7	0.04	-7.2	-36.3	46.9	15.7	0.17	-4.2	-21.3	42.8
	CSN	2.06	1.06	0.78	-1.0	-48.3	48.4	1.02	0.78	-1.04	-50.7	50.8
SO ₄ ²⁻ (µg m ⁻³)	IMPROVE	0.79	0.49	0.95	-0.3	-37.4	38.9	0.49	0.95	-0.3	-38.5	39.9
	CSN	2.37	2.36	0.79	-0.01	-0.3	25.8	2.89	0.81	0.52	21.7	37.8
NO ₃ ⁻ (µg m ⁻³)	IMPROVE	0.73	0.83	0.87	0.1	13.3	40.9	1.06	0.90	0.33	44.6	54.4
	CSN	1.30	0.92	0.80	-0.38	-29.4	30.5	1.03	0.81	-0.27	-21.0	24.1
NH ₄ ⁺ (µg m ⁻³)	CSN	0.69	0.75	0.18	0.06	8.7	58.5	0.79	0.24	0.1	14.2	58.0
	IMPROVE	0.17	0.23	0.80	0.06	40.8	59.2	0.25	0.84	0.09	53.4	65.6
EC (µg m ⁻³)	IMPROVE	0.65	0.74	0.65	0.09	13.0	55.7	0.8	0.67	0.15	23.1	56.4
	CSN	3.05	3.27	0.01	0.22	7.2	53.2	3.49	0.0	0.44	14.4	55.8
TC (µg m ⁻³)	IMPROVE	0.53	0.62	0.75	0.09	17.5	51.3	0.68	0.78	0.15	28.1	52.6
	MOPITT	1.96	1.56	0.70	-0.4	-20.5	21.6	1.57	0.69	-0.39	-19.8	21.1
Col. CO (10 ¹⁸ mole. cm ⁻³)	OMI	26.4	27.6	0.78	1.2	4.7	14.0	28.0	0.19	1.6	5.9	14.3
Col. NO ₂ (10 ¹⁵ mole. cm ⁻³)	SCIAMACHY	1.55	1.55	0.86	0.04	0.3	33.5	1.53	0.87	-0.02	-1.2	33.1
Col. HCHO (10 ¹⁵ mole. cm ⁻³)	SCIAMACHY	4.87	2.48	0.29	-2.39	-49.0	50.1	2.53	0.28	-2.34	-48.0	49.2

Table 4. The 5-year average performance statistics for chemical variables between two-way WRF-CMAQ and offline CMAQ simulations in summer, 2008-2012.

Variables	Datasets	Mean Obs	Two-way WRF-CMAQ					Offline CMAQ				
			Mean Sim	R	MB	NMB (%)	NME (%)	Mean Sim	R	MB	NMB (%)	NME (%)
Max 8-hr O ₃ (ppb)	AQS	47.9	53.0	0.66	5.1	10.6	13.2	54.8	0.66	6.8	14.2	15.6
	CASTNET	47.2	45.8	0.66	-1.4	-3.0	11.5	47.3	0.68	0.1	0.2	10.5
PM _{2.5} (µg m ⁻³)	CSN	11.4	9.9	0.74	-1.5	-13.2	20.5	9.8	0.71	-1.6	-14.0	20.8
	IMPROVE	6.19	4.52	0.88	-1.66	-26.9	31.2	4.78	0.86	-1.41	-22.8	28.9
PM ₁₀ (µg m ⁻³)	AQS	26.7	14.5	0.03	-12.2	-45.8	50.7	16.2	0.07	-10.5	-39.4	48.6
	CSN	2.86	2.57	0.91	-0.29	-10.2	15.1	2.34	0.91	-0.52	-18.1	19.5
SO ₄ ²⁻ (µg m ⁻³)	IMPROVE	1.40	1.11	0.98	-0.29	-20.9	21.3	1.08	0.98	-0.31	-22.5	22.6
	CSN	0.49	0.71	0.54	0.22	45.2	70.6	0.77	0.59	0.28	57.2	76.8
NO ₃ ⁻ (µg m ⁻³)	IMPROVE	0.20	0.19	0.6	-0.01	-4.7	71.4	0.22	0.63	0.02	10.3	72.2
	CSN	0.91	0.94	0.86	0.03	3.3	22.4	0.88	0.85	-0.03	-3.6	20.1
EC (µg m ⁻³)	CSN	0.56	0.79	0.56	0.23	41.0	56.3	0.79	0.55	0.23	41.9	55.5
	IMPROVE	0.20	0.24	0.56	0.04	20.4	58.8	0.26	0.52	0.06	27.9	63.0
OC (µg m ⁻³)	IMPROVE	1.37	0.70	0.31	-0.67	-49.2	54.0	0.75	0.28	-0.62	-45.4	52.4
	CSN	2.85	2.17	0.54	-0.67	-23.6	29.3	2.19	0.5	-0.65	-22.9	29.7
TC (µg m ⁻³)	IMPROVE	0.88	0.61	0.56	-0.27	-30.5	47.6	0.66	0.53	-0.23	-25.6	47.6
	MOPITT	1.82	1.32	0.75	-0.5	-27.8	27.8	1.32	0.54	-0.5	-27.3	27.3
Col. CO (10 ¹⁸ mole. cm ⁻³)	OMI	35.0	32.2	0.87	-2.8	-8.0	9.0	32.4	0.85	-2.6	-7.3	8.6
Col. NO ₂ (10 ¹⁵ mole. cm ⁻³)	SCIAMACHY	1.08	0.78	0.81	-0.3	-27.8	38.0	0.78	0.80	-0.3	-27.5	38.1
Col. HCHO (10 ¹⁵ mole. cm ⁻³)	SCIAMACHY	5.81	6.71	0.82	0.9	15.0	22.5	6.82	0.82	1.01	17.4	23.5

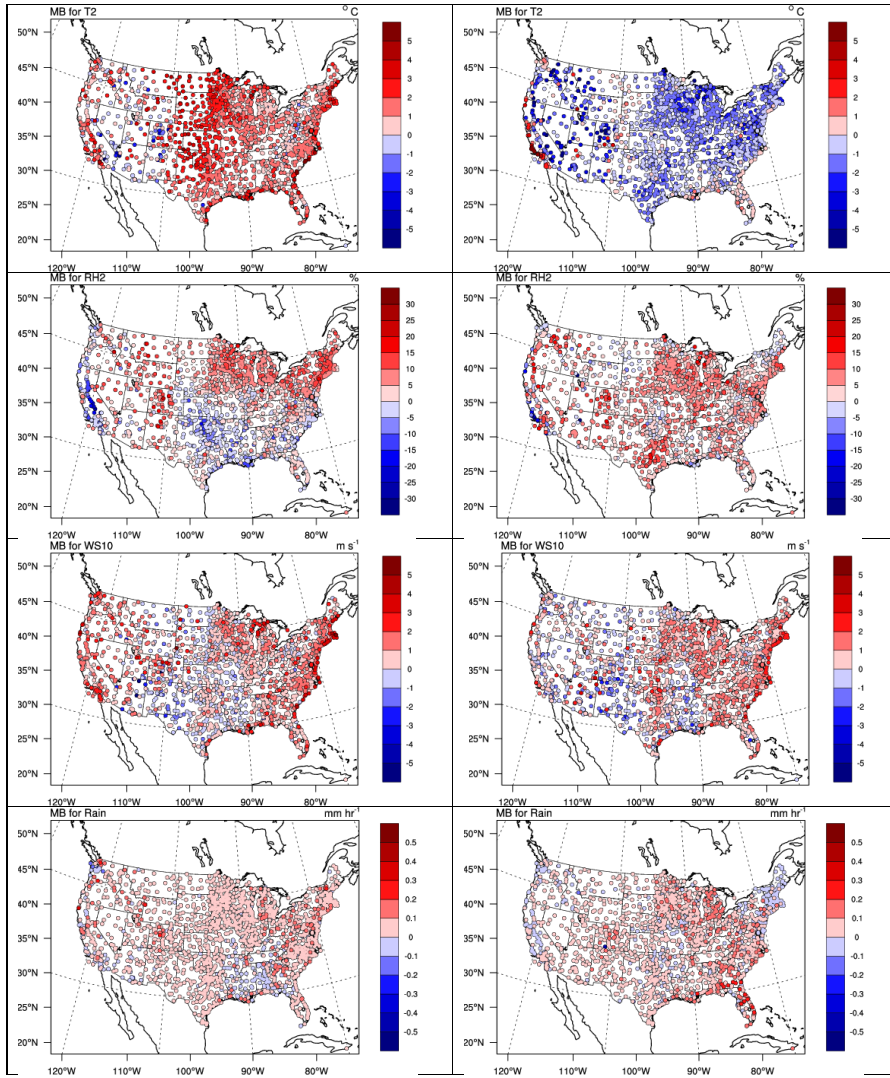


Figure 1. Spatial distributions of 5-year average MBs for 2-m temperature (T2), 2-m relative humidity (RH2), 10-m wind speed (WS10), and hourly precipitation from NCD for two-way WRF-CMAQ in winter (left panel) and summer (right panel), 2008-2012.

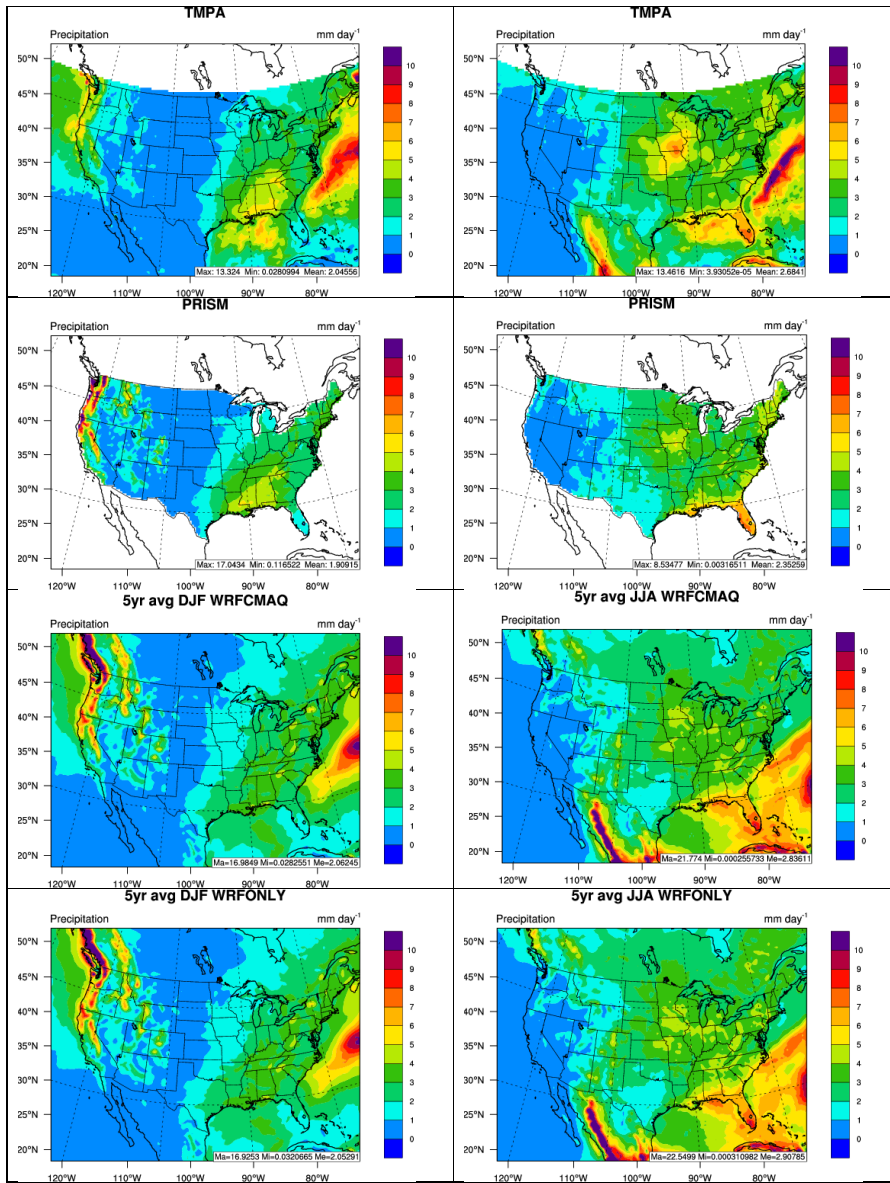


Figure 2. Spatial distributions of 5-year average of daily precipitation from TMPA, PRISM, two-way WRF-CMAQ, and WRF-only (from top to bottom) in winter (left panel) and summer (right panel), 2008-2012.

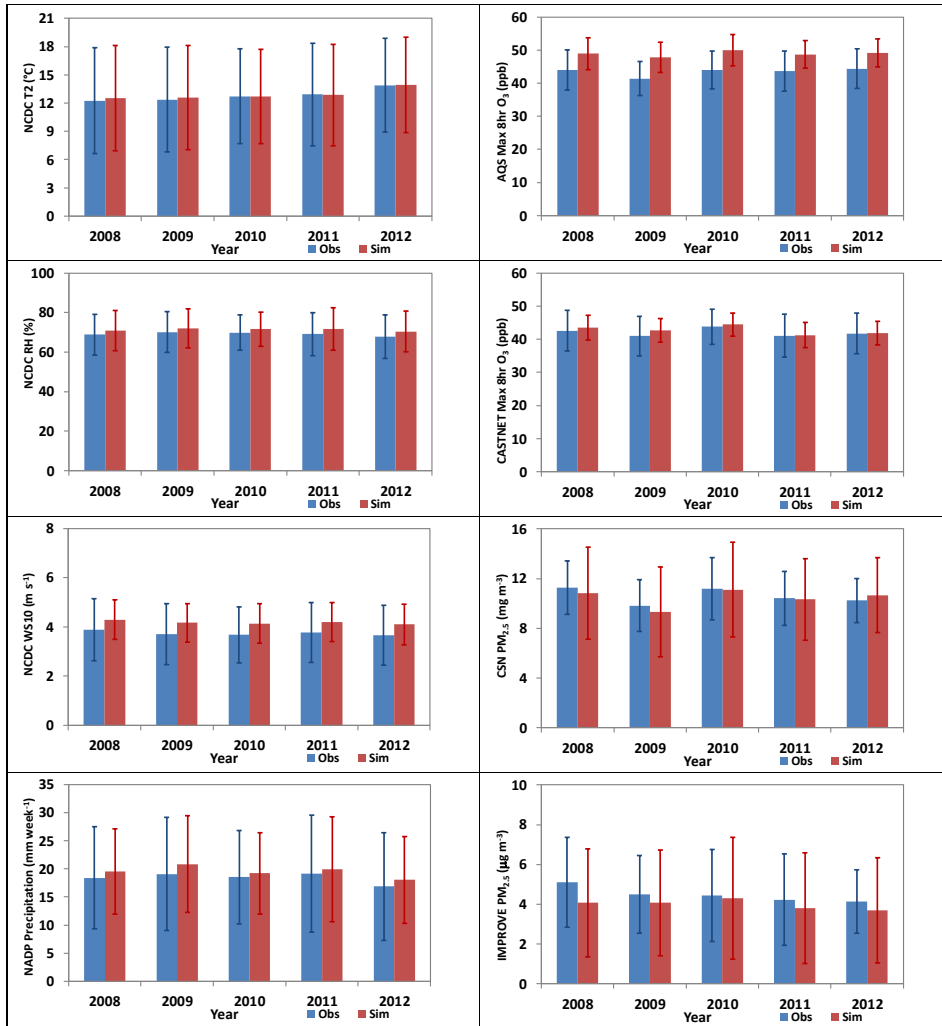


Figure 3. Bar charts for annual average observations and simulations (standard deviations are displayed as the error bars) from two-way WRF-CMAQ for major meteorological variables (left panel) and chemical species (right panel) in 2008-2012.

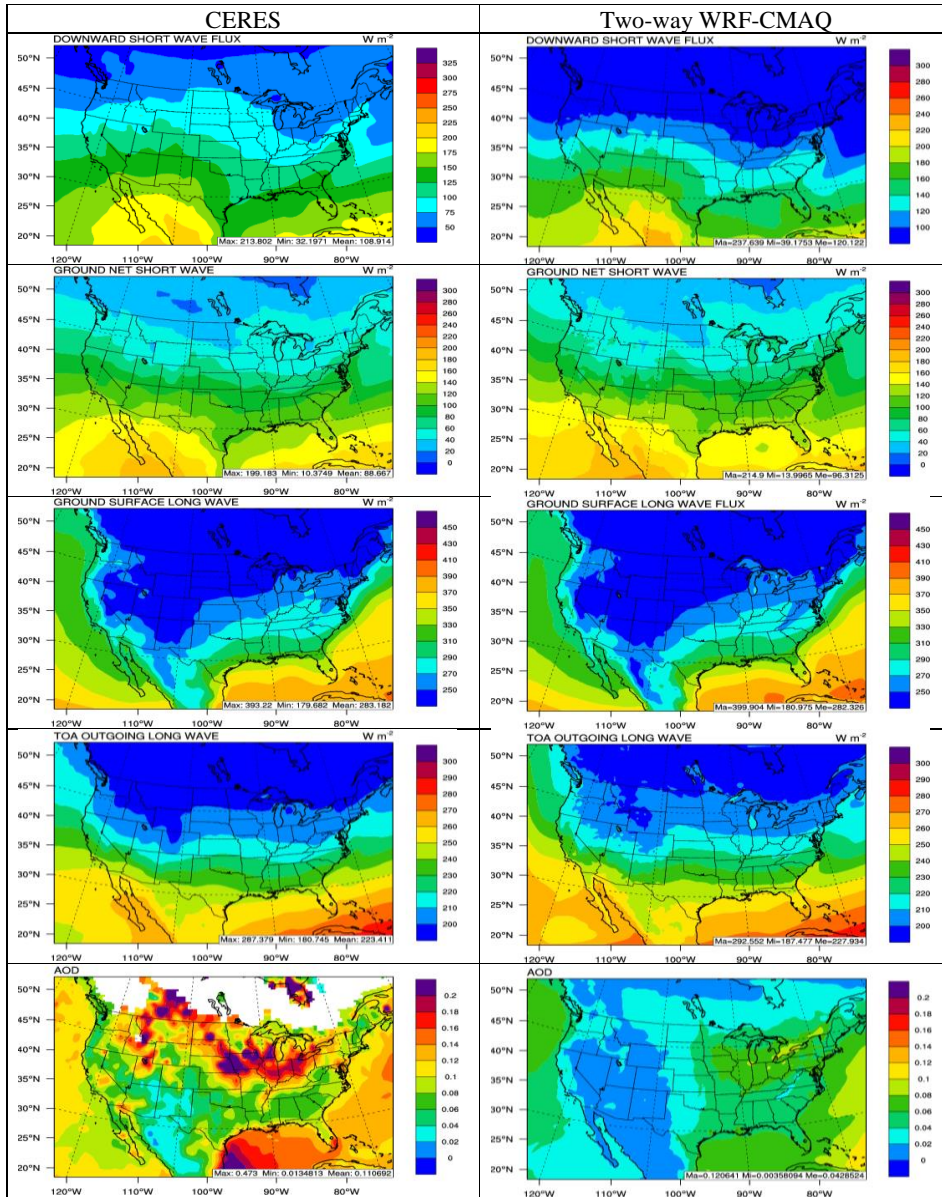


Figure 4. Spatial distribution of 5-year average major radiation variables (from top to bottom: SWDOWN, GSW, GLW, OLR, and AOD) between CERES observations (left panel) vs. two-way WRF-CMAQ (right panel) in winter, 2008-2012.

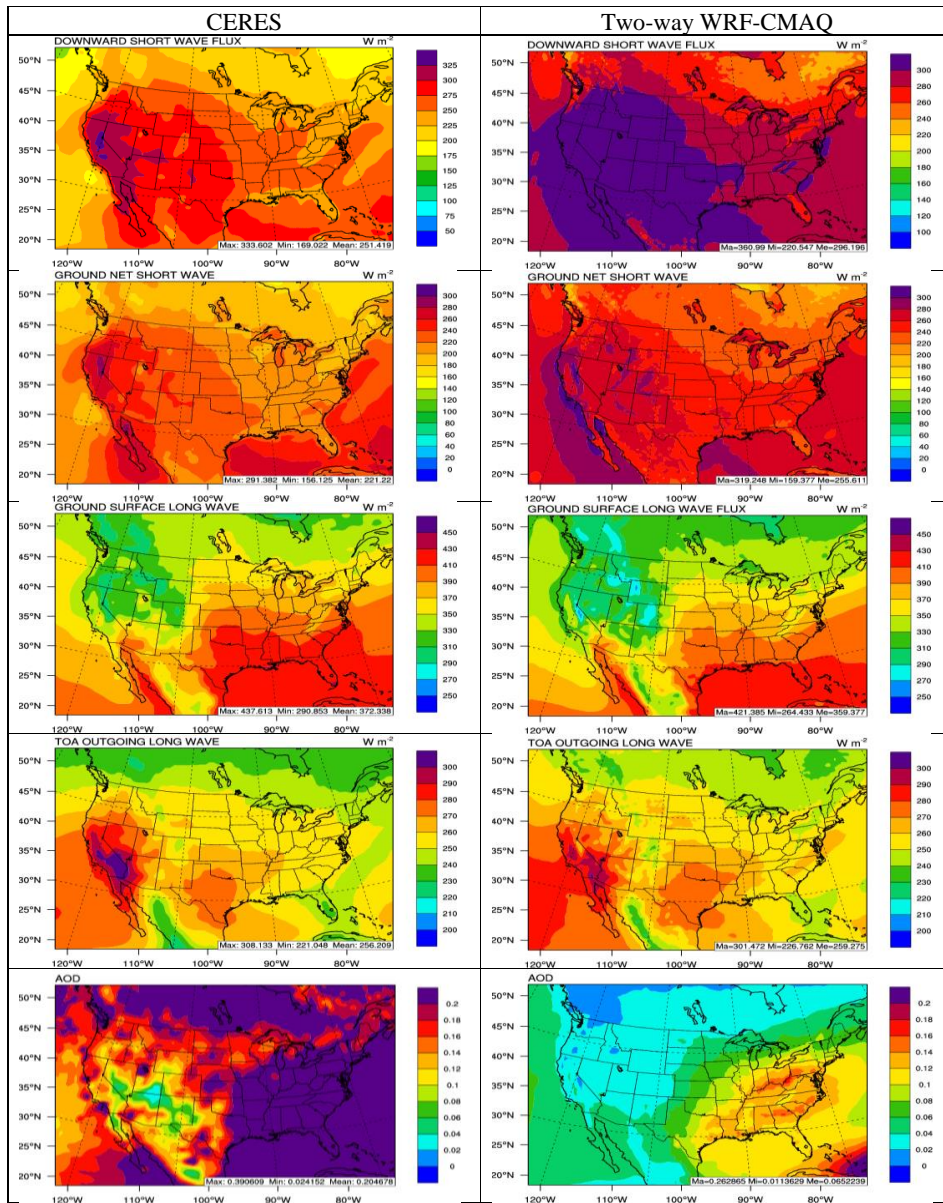


Figure 5. Spatial distribution of 5-year average major radiation variables (from top to bottom: SWDOWN, GSW, GLW, OLR, and AOD) between CERES observations (left panel) vs. two-way WRF-CMAQ (right panel) in summer, 2008-2012.

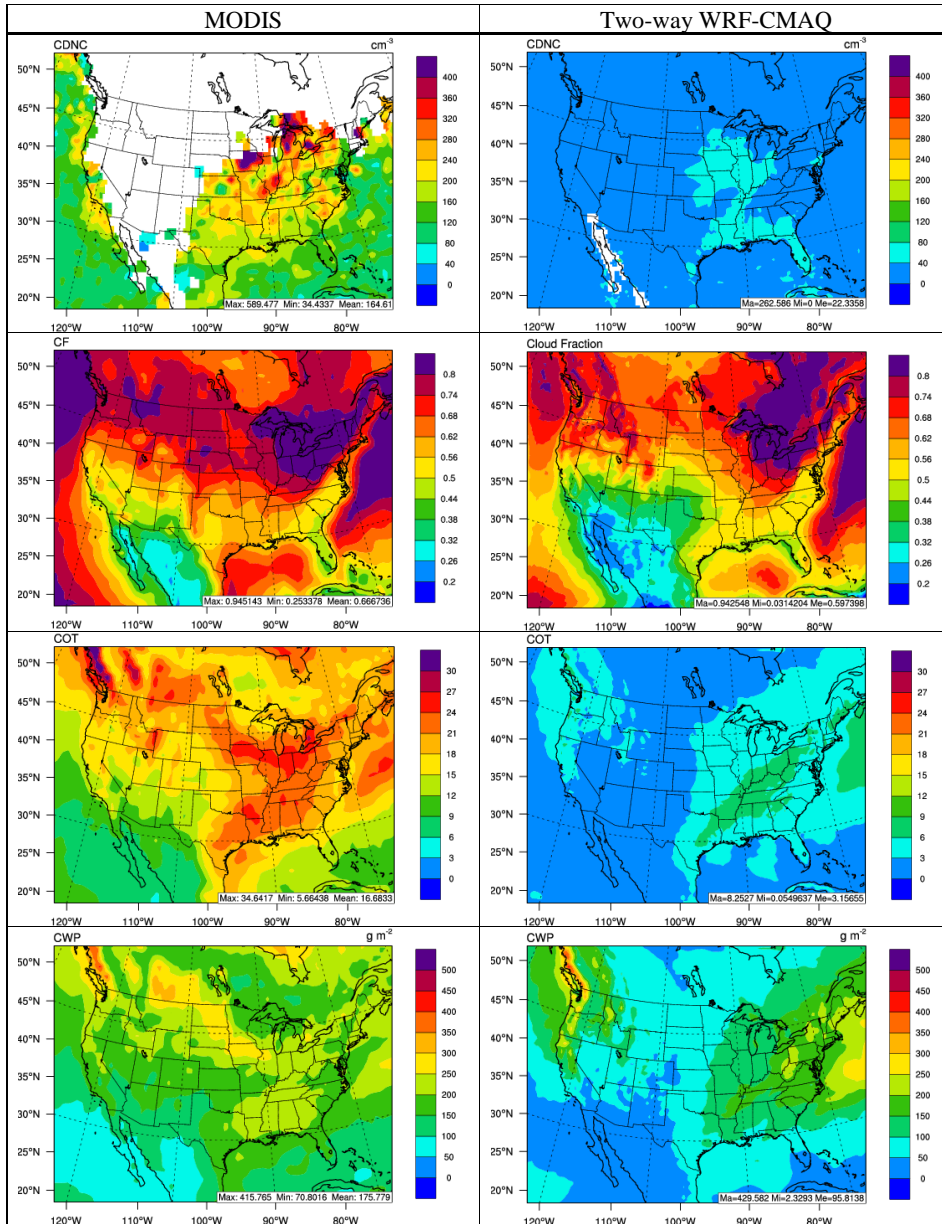


Figure 6. Spatial distribution of 5-year average major cloud variables (from top to bottom: CDNC, CF, COT, and CWP) between MODIS observations (left panel) vs. two-way WRF-CMAQ (right panel) in winter, 2008-2012.

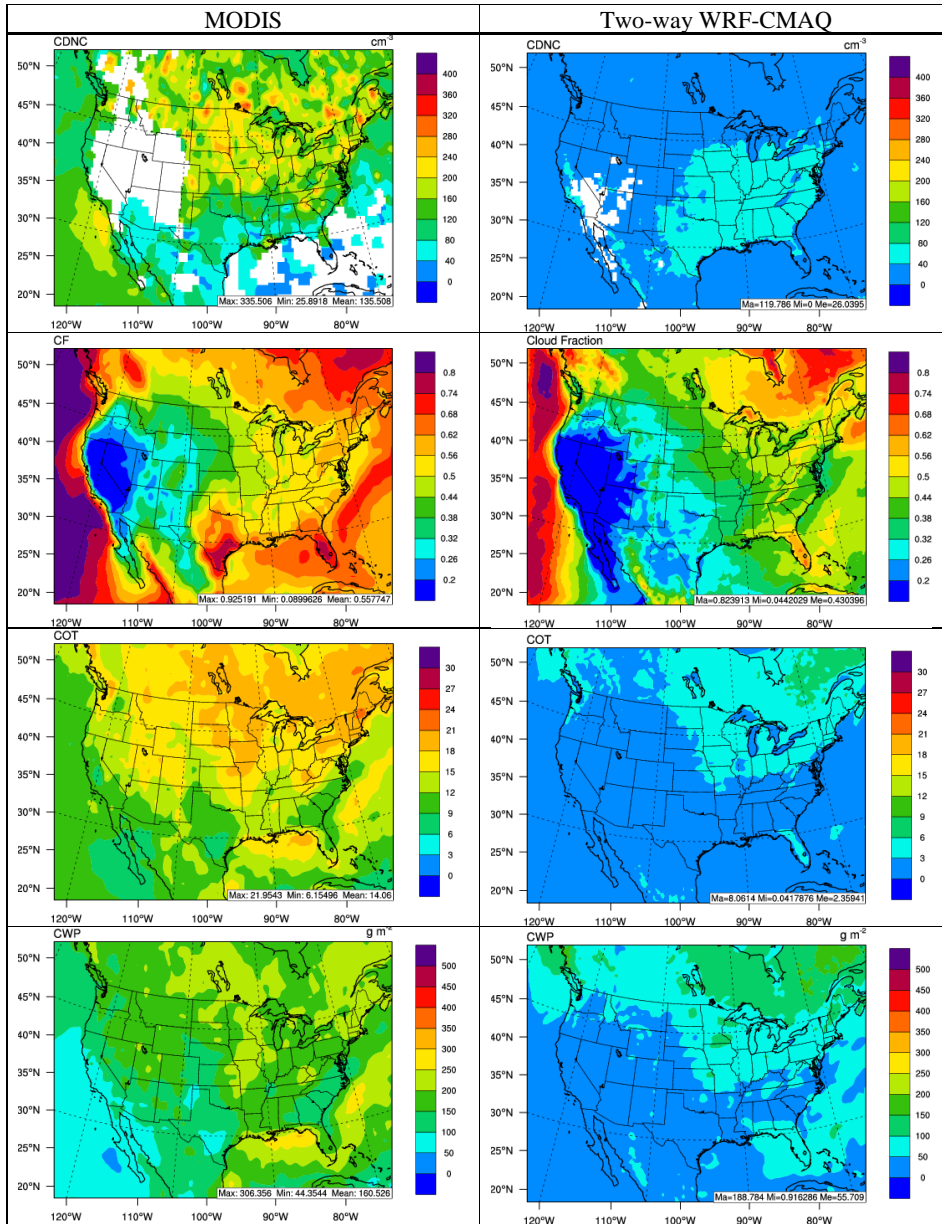


Figure 7. Spatial distribution of 5-year average major cloud variables (from top to bottom: CDNC, CF, COT, and CWP) between MODIS observations (left panel) vs. two-way WRF-CMAQ (right panel) in summer, 2008-2012.

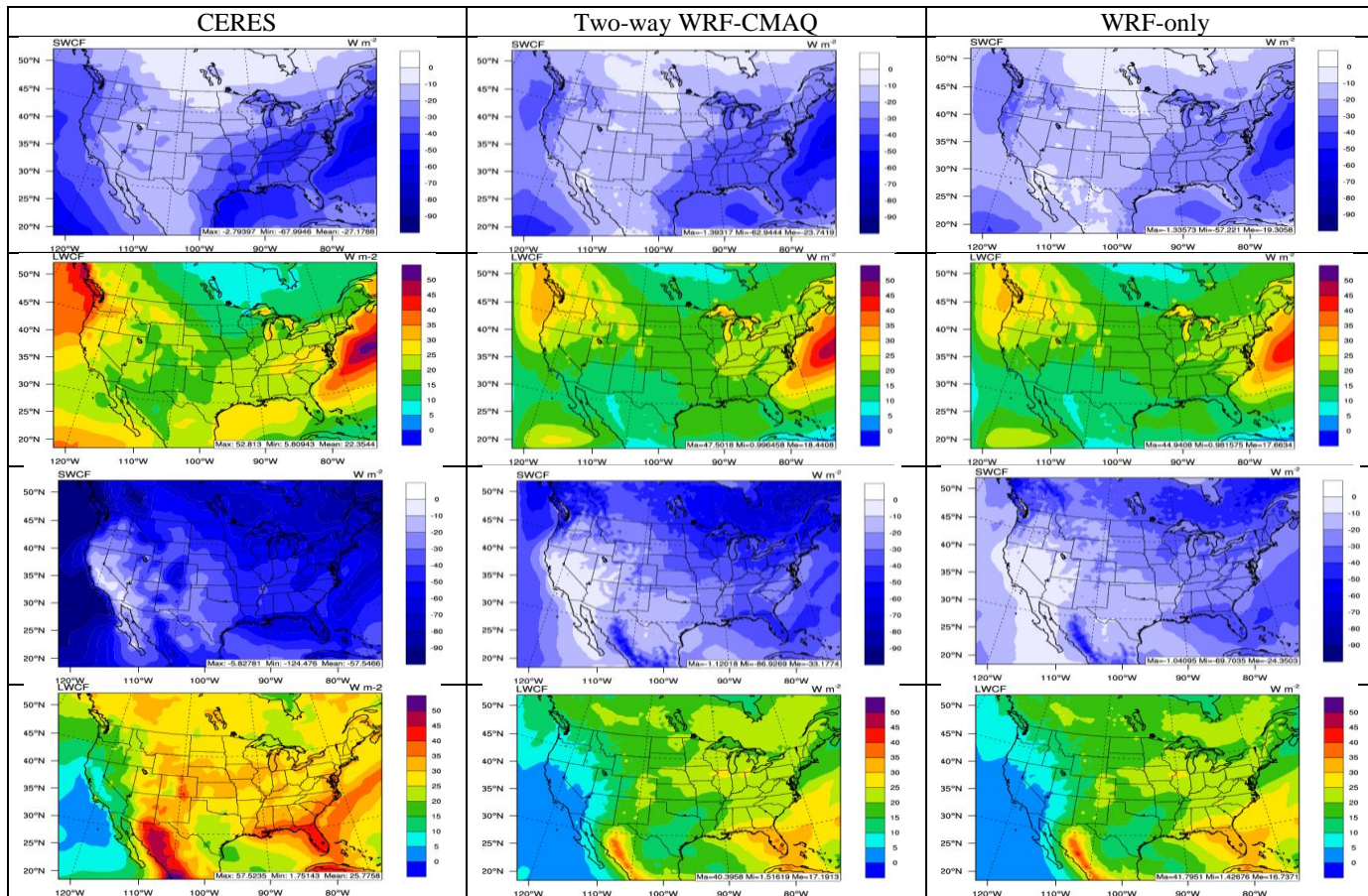


Figure 8. Spatial distribution of 5-year average SWCF in winter, LWCF in winter, SWCF in summer, and LWCF in summer (from top to bottom) between CERES observations (left panel) vs. two-way WRF-CMAQ (center panel) and WRF-only (right panel) in 2008-2012.

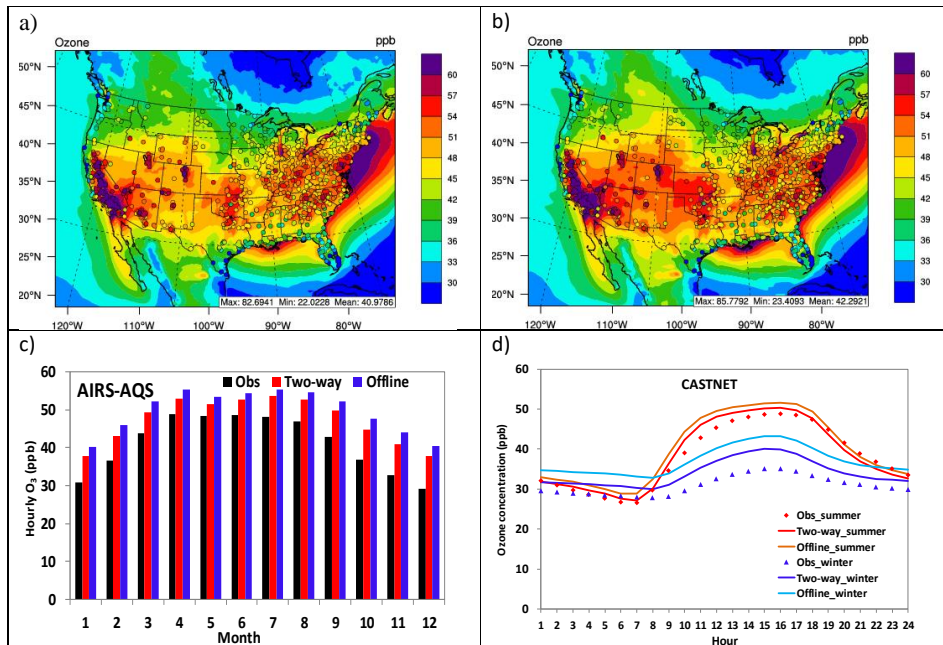


Figure 9. Spatial distributions of 5-year averaged max 8-h O_3 in summer overlaid with observations from AIRS-AQS and CASTNET for a) two-way WRF-CMAQ and b) offline CMAQ; c) bar chart for 5-year average monthly O_3 between observations (black bar), two-way WRF-CMAQ (red bar), and offline CMAQ (blue bar); and d) diurnal plots of observed (dots) vs. simulated (lines) hourly O_3 concentrations against CASTNET for winter (cold colors) and summer (warm colors) in 2008-2012.

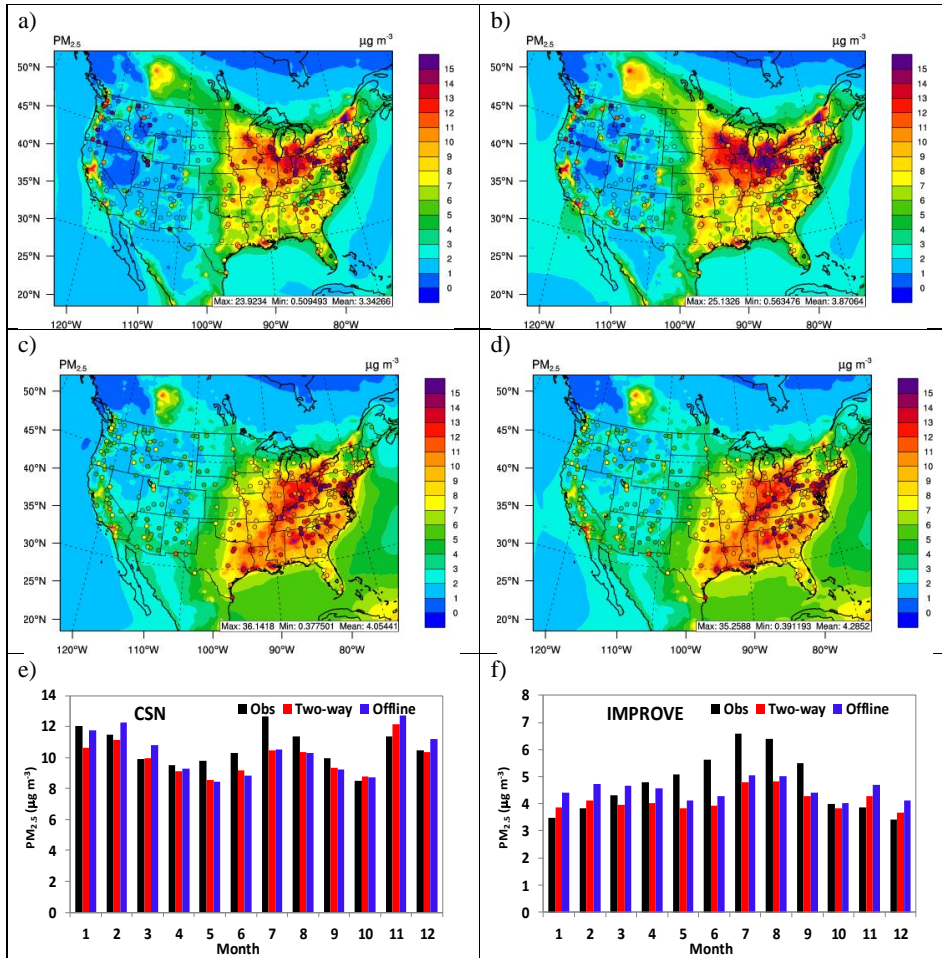


Figure 10. Spatial distributions of 5-year averaged daily PM_{2.5} overlaid with observations from CSN and IMPROVE for two-way WRF-CMAQ in a) winter and c) summer and offline CMAQ in b) winter and d) summer; bar charts for 5-year average monthly PM_{2.5} between observations (black bar), two-way WRF-CMAQ (red bar), and offline CMAQ (blue bar) over e) CSN and f) IMPROVE in 2008-2012.

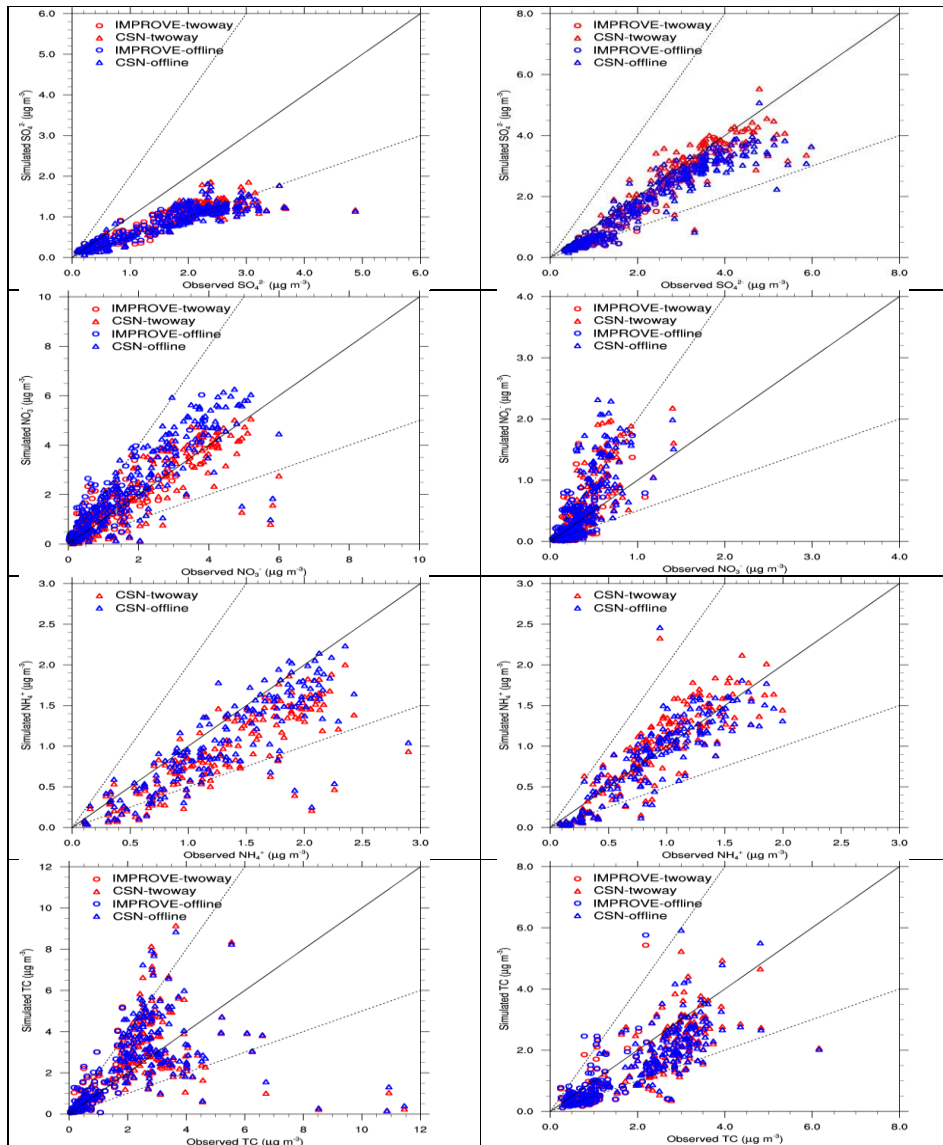


Figure 11. Scatter plots of 5-year averaged PM_{2.5} constituents for SO₄²⁻, NO₃⁻, NH₄⁺, and TC (from top to bottom) between observations and simulations of two-way WRF-CMAQ (red color) and offline CMAQ (blue) in winter (left panel) and summer (right panel), 2008-2012.

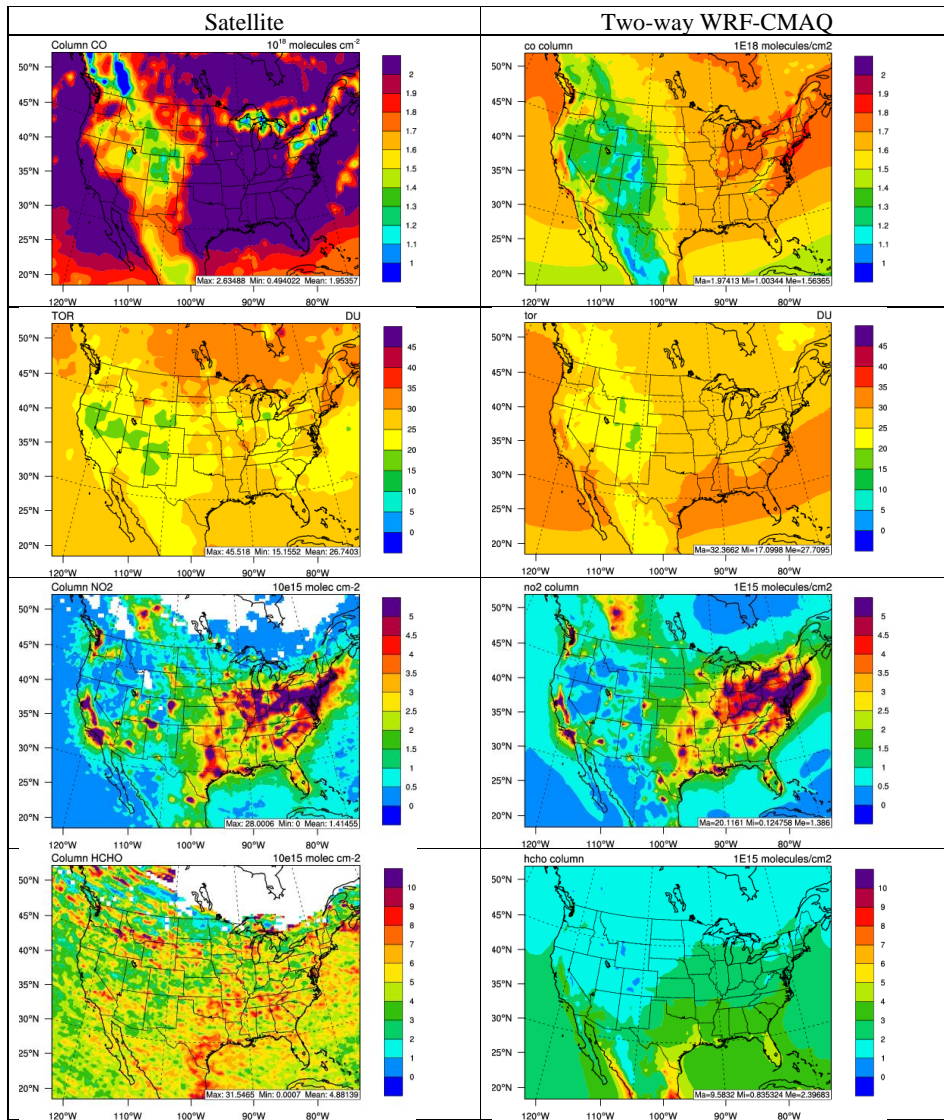


Figure 12. Spatial distribution of 5-year average column abundances (from top to bottom: column CO, TOR, column NO₂, and column HCHO) between various satellite observations (left panel) vs. two-way WRF-CMAQ (right panel) in winter, 2008-2012.

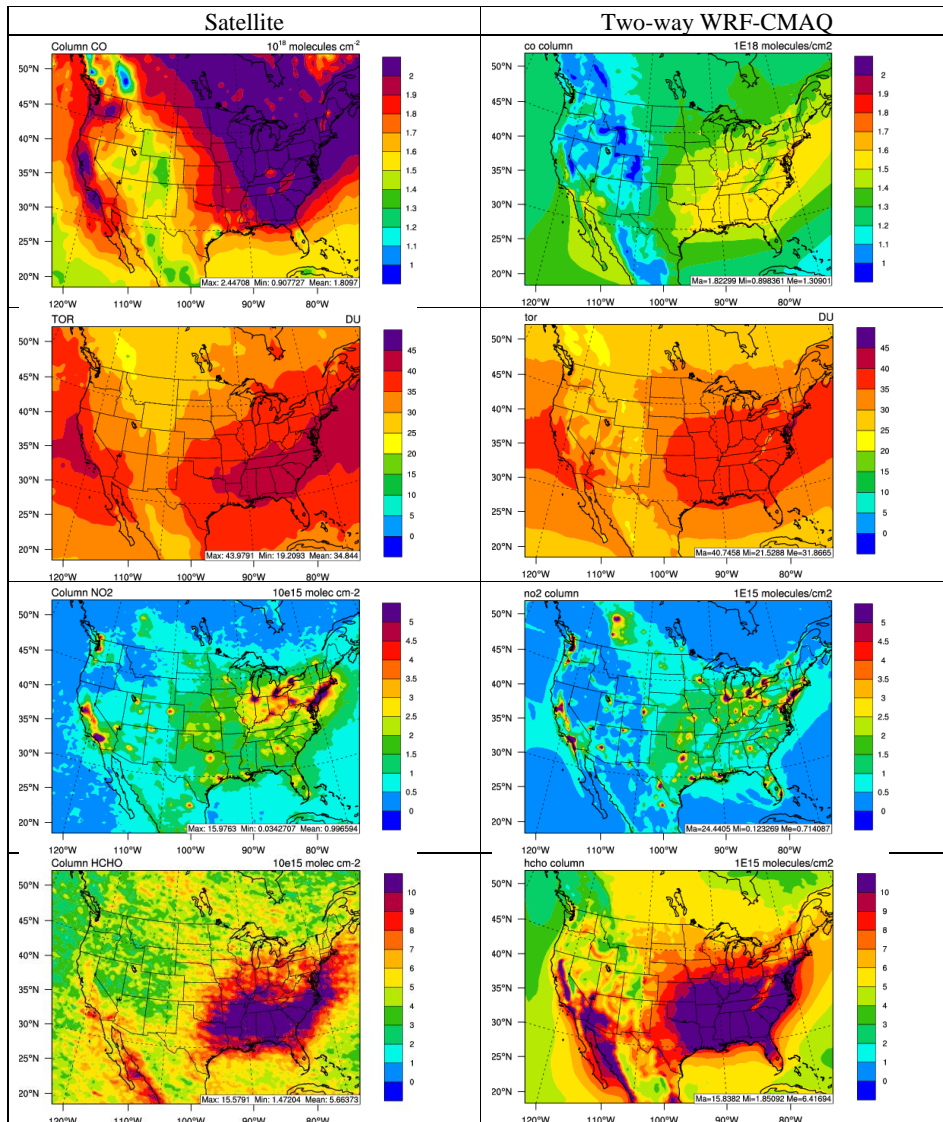


Figure 13. Spatial distribution of 5-year average column abundances (from top to bottom: column CO, TOR, column NO₂, and column HCHO) between various satellite observations (left panel) vs. two-way WRF-CMAQ (right panel) in summer, 2008-2012.

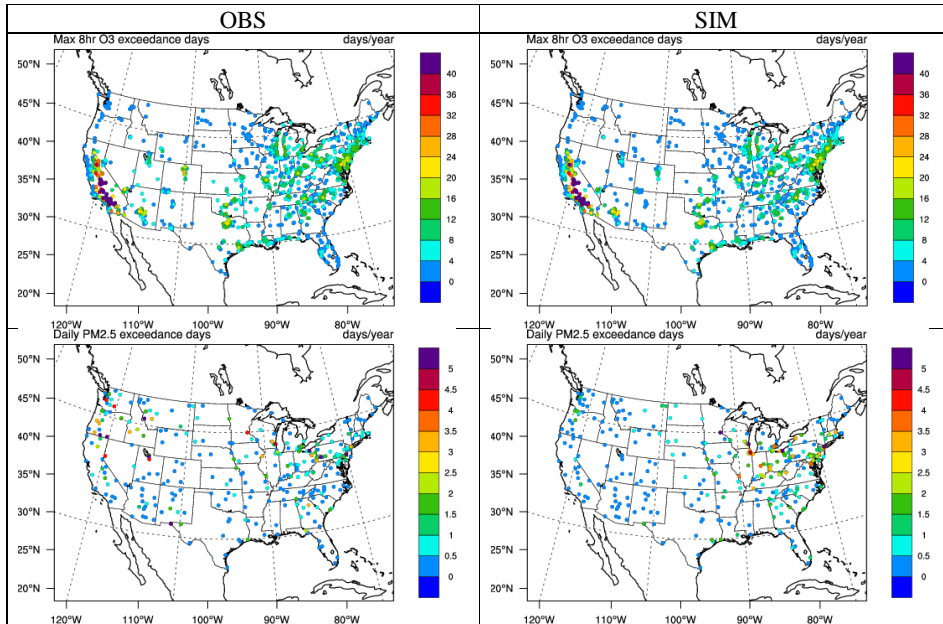


Figure 14. The spatial distribution of 5-year average annual exceedance days of max 8-h O_3 and daily $PM_{2.5}$ between observations (O_3 over the AIRS-AQS/CASTNET network and $PM_{2.5}$ over the IMPROVE/CSN network) and two-way WRF-CMAQ in 2008-2012.

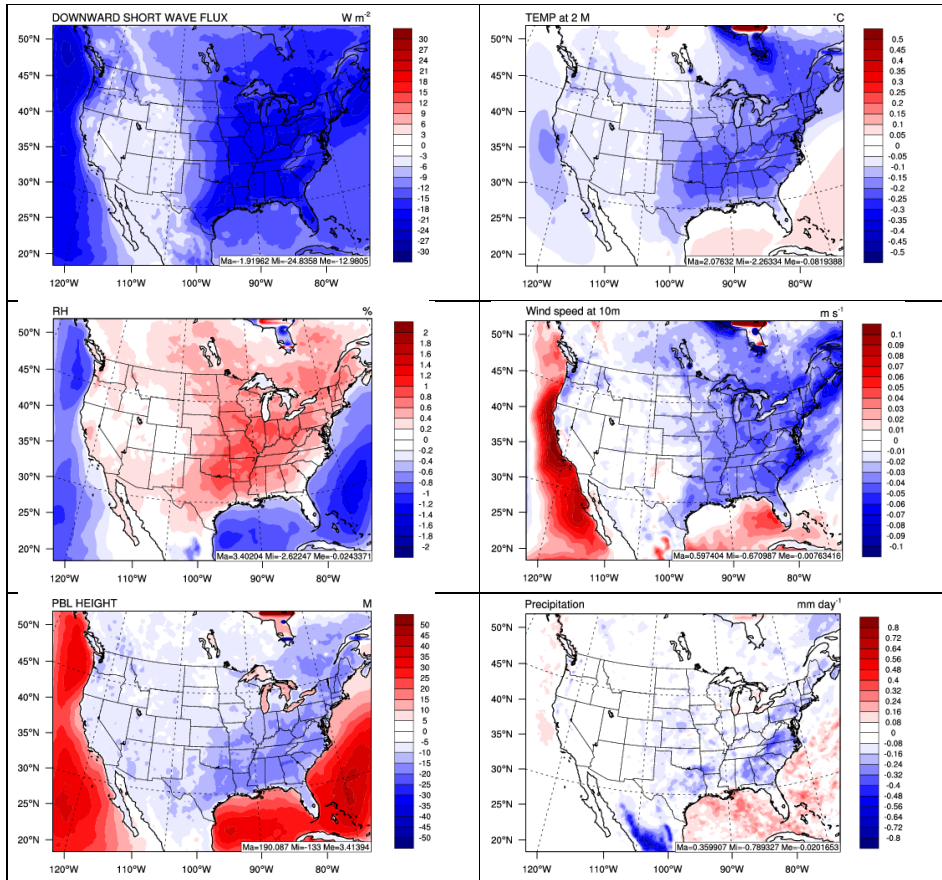


Figure 15. Spatial difference plots (two-way WRF-CMAQ - WRF-only) for major meteorological variables between two-way WRF-CMAQ and WRF-only in 2008-2012.

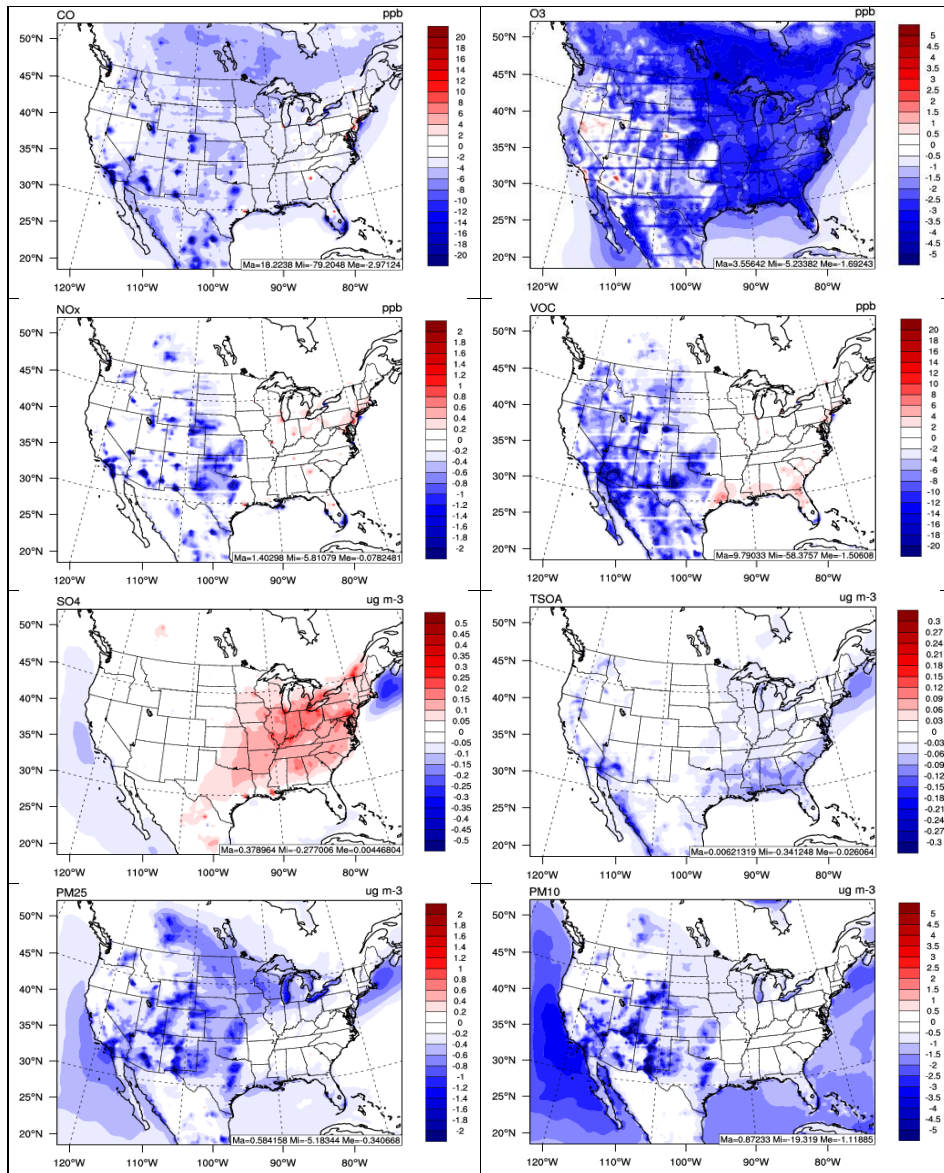


Figure 16. Spatial difference plots (two-way WRF-CMAQ - offline CMAQ) for major chemical species between two-way WRF-CMAQ and offline CMAQ in 2008-2012.